Poplar Wood Torrefaction: Kinetics, Thermochemistry and Implications

*(submitted to **Renewable and Sustainable Energy Reviews**)*

Meiyun Chai [a], Li Xie [a], Xi Yu [b], Xingguang Zhang [c], Yang Yang [b], Md. Maksudur Rahman [a], Paula H. Blanco [b], Ronghou Liu [a], Anthony V. Bridgwater [b], Junmeng Cai [a,*]

[a] Biomass Energy Engineering Research Center, School of Agriculture and Biology, Shanghai Jiao Tong University, 800 Dongchuan Road, Shanghai 200240, People's Republic of China

[b] Energy & Bioproducts Research Institute (EBRI), Aston University, Aston Triangle, Birmingham B4 7ET, United Kingdom

[c] Department of Chemistry, School of Science, University of Shanghai for Science and Technology, 516 Jungong Road, Shanghai 200093, People's Republic of China

* Corresponding author: Junmeng Cai. E-mail address: jmcai@sjtu.edu.cn; Tel.: +86-21-34206624; Website: http://biofuels.sjtu.edu.cn.

Abstract

In this paper, a torrefaction kinetic model for poplar wood torrefaction coupling with an existing two-step kinetic model was presented. The presented torrefaction kinetic model satisfactorily fitted the experimental thermogravimetric analysis (TGA) data for poplar wood torrefaction; it also provided a coherent description of the evolution of torrefaction volatiles and solid products in terms of a set of identifiable chemical components and elemental compositions respectively. A comprehensive torrefaction thermochemical model was proposed to describe the thermochemical performance of poplar wood torrefaction processes. The results from the developed torrefaction kinetic and thermochemical model showed that (1) high temperature increases the evolution rate of torrefaction products, and favors the formation of torrefaction volatiles; (2) heating rate has a slight effect on evolution for torrefaction process; (3) mass and energy yields of torrefaction products are significantly influenced by both torrefaction temperature and residence time; (4) heat of torrefaction reaction is mostly endothermic with a relatively small amount (less than 10% of the raw material energy content); (5) for the overall torrefaction processes, the sensible and latent energy of torrefaction products accounts for 5 – 18% of the total energy input and the remaining energy input transfers into the energy contents of products. This work provides a theoretical guidance for future evaluation and optimization of a torrefaction system, and thereafter for the industrial application of thermochemical conversion of woody biomass.

Keywords: biomass; torrefaction; thermogravimetric analysis (TGA); kinetics; thermochemistry; energy balance.

Graphical abstract
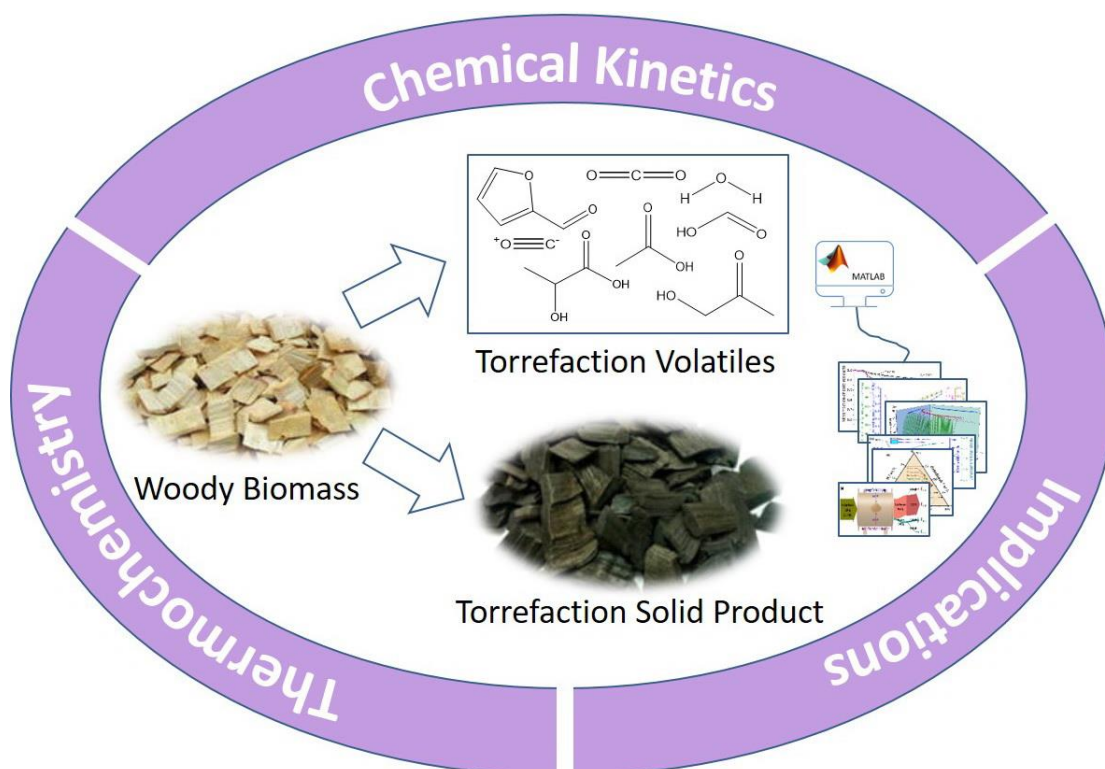
List of abbreviations

Symbols	Nomenclature	Units
A	Frequency factor	s^{-1}
C	Mass fraction	wt.%
E	Activation energy	kJ mol^{-1}
P	Power	kw kg^{-1}
Q	Sensible heating energy	kJ kg^{-1}
c_P	Specific heat capacity	J kg^{-1} K^{-1}
$E_{C\text{-}SP}$	Energy content of solid products	MJ kg^{-1}
$E_{C\text{-}V}$	Energy content of volatiles	MJ kg^{-1}
$E_{SL\text{-}V}$	Sensible and latent energy of volatiles	MJ kg^{-1}
$E_{S\text{-}SP}$	Sensible energy of solid products	MJ kg^{-1}
$\Delta_i H^{\theta}$	Standard enthalpies of formation	kJ kg^{-1}
ΔH_r	Heat of reaction	kJ kg^{-1}
N_v	Number of the components in the torrefaction	dimensionless

	volatiles	
R^2	Coefficients of determination	dimensionless
EC	Elemental contents of C	kg kg^{-1}
EH	Elemental contents of H	kg kg^{-1}
EN	Elemental contents of N	kg kg^{-1}
EO	Elemental contents of O	kg kg^{-1}
ES	Elemental contents of S	kg kg^{-1}
HHV	Higher heating value	MJ kg^{-1}
m	Mass of the biomass	kg
SIP	Solid Intermediate Products	dimensionless
SP	Solid products, the sum of SIP and TB	dimensionless
SR	Solid residual, the sum of unreacted WB, SIP and TB	dimensionless
T	Temperature	ºC or K
t	Time	s
TB	Torrefied biomass	dimensionless
TGA	Thermogravimetric analysis	dimensionless
V	Volatile	dimensionless
Va	Volatile A	dimensionless
Vb	Volatile B	dimensionless
WB	Woody biomass	dimensionless
β	Heating rate	ºC min^{-1}
η	Energy yield	%

Subscripts

a	Startup
f	Final
r	Residence
0	Initial

1 Introduction

The direct use of lignocellulosic biomass (e.g., agricultural and forest residues) as fuel is inefficient because of its poor energy efficiency (e.g., low heating value, high moisture content, hygroscopic nature, low density and polymorphism, causing high costs during transportation, handling and storage) [1-3]. Lignocellulosic biomass contains three major biopolymer components: hemicellulose, cellulose and lignin [2]. Cellulose is an organic polysaccharide consisting of a linear chain of several hundred to thousands of β poly linked D-glucose units [4]. The predominant form of hemicellulose is xylan, a pentose polysaccharide consisting of D-xylose units with 1-β-4 linkages. Hydroxyphenyl, guaiacyl, and syringyl bonded together randomly by the ether bond (β-O-4, α-O-4, and γ-O-4) and the carbon-carbon bond (5-5, β-1, and β-5)

constitute lignin, whose thermal degradation temperature range is wide, because of its inhomogeneous distribution of molecular weight [5]. Lignocellulosic biomass can be converted to produce heat, chemicals, materials and/or fuels through thermal conversion processes such as pyrolysis [6]. Pyrolysis is the thermal decomposition of biomass in the absence of oxygen [7], which has attracted immense attention because it can convert biomass into high energy-dense liquid fuel with the potential of substituting petroleum fuels [8].Torrefaction is a mild pyrolysis process of biomass, and it is typically carried out in a temperature range between 200 and 300 ℃ [9]. Water contained in biomass can be evaporated in this temperature range. During torrefaction, different biomass components show different thermal decomposition behaviors [10]: the hemicellulose components decompose extensively, whereas cellulose and lignin show limited decomposition because hemicelluloses consist of shorter and branched chains compared with cellulose and lignin [11]. According to Ru et al. [12], dehydration of hydroxyls, deacetylation of O-acetyl branches, and cleavage of ether linkages occur simultaneously during biomass torrefaction, which are related to thermal decomposition of hemicelluloses. Torrefaction can remove some light volatiles from biomass, yielding a torrefied biomass with lower content of oxygen and higher content of carbon than those of the raw biomass [13, 14].Torrefaction can improve the quality of solid products by releasing oxygen-containing components from torrefed gaseous (e.g., CO_2, H_2O and CO) and liquid products (e.g., acids, phenols, furans and ketones) [15] or the breakage of oxygen-containing functional groups or linkages, such as β-O-4 bonds, aliphatic-OH and -COOH, aromatic-OCH_3 [16]. The energy content and density of torrefied biomass are higher than those of raw biomass as torrefaction changes in elemental and structural compositions of biomass [17, 18]. Hemicelluloses can create structural linkages within biomass [19], their decomposition during torrefaction yields torrefied biomass with lower strength and easier grindability [20-22]. Torrefied biomass shows improved hydrophobicity; therefore, it can be stored stable over an extended period of time with a reduced risk of biological deterioration [23, 24]. Besides improving physicochemical properties of biomass, torrefaction can also improve its thermal conversional performance. Torrefaction can result in lower yields of acids and furfural in the pyrolytic product distribution when torrefied biomass is further processed by pyrolysis [25, 26]. Torrefaction can improve the overall gasification efficiency up to 72.6% for torrefied willow wood compared with 68.6% from gasification of raw willow wood according to Prins et al. [27]. Similar results have been reported from the gasification of torrefied tomato peels [28], and oil palm biomass [29]. In addition, torrefaction treatment can change biomass properties to provide a better fuel quality for combustion [30-32]. **Table 1** compares the physicochemical properties of biomass and torrefied biomass.

Table 1. Qualitative physicochemical properties of raw biomass and torrefied biomass

4

	Raw biomass	Torrefied biomass
Moisture content (%)	4 – 15	~0
Oxygen content (%)	40 – 50	30 – 40
Heating value (MJ kg^{-1})	10 – 19	17 – 30
Energy density	~1	1.25 – 1.5
Hydroscopic properties	Hygroscopicity	Hydrophobicity
Particle sizes	Non-uniform	Uniform
Biological degradation	Fast	Slow
Thermochemical conversion performance	Weak	Strong
Handling and transport cost (RMB/t)	500	200

The kinetics of biomass torrefaction is fundamental for the prediction of thermal decomposition kinetic characteristics under different torrefaction conditions and is helpful for the design and scale-up of torrefaction systems and the optimization of torrefaction processes [33, 34]. Some studies have been performed on the torrefaction kinetics of different biomass feedstocks and/or their individual lignocellulosic components. Swiechowski et al. [35] used an empirical model in the form of an exponential function to describe the isothermal torrefaction of oxytree pruned residues. According to our previous paper [36], the empirical model has only statistical meaning and some theoretical drawbacks in describing the kinetics of biomass torrefaction. Chen et al. [37] used a one-step kinetic model to analyze the torrefaction kinetics of pine, fir and spruce and found that it could accurately predict the torrefaction processes over long residence time (from 0.5 to 3 hours or more) but failed over short residence time (5 – 20 minutes). The model was found to be used in the torrefaction kinetic analysis of wheat straw [33] and beech wood [36]. However, the one-step kinetic model was not able to fit the experimental results of biomass torrefaction satisfactorily, as the competitive formation of volatile and solid products during torrefaction was not considered. Bach et al. [38] proposed a three-independent-parallel-reaction model to analyze the torrefaction kinetics of Norway spruce branches. In the model, three parallel reactions corresponded to the thermal decomposition of lignocellulosic components: hemicellulose, cellulose, and lignin. The nth-order reaction models with different Arrhenius parameters and reaction orders were used to describe three independent parallel reactions. Therefore, the three-independent-parallel-reaction model is the weighted sum of three reactions. However, hemicellulose can decompose almost completely, while cellulose only partially decomposes and lignin does not hardly decompose. Therefore, the three-independent-parallel-reaction model is not appropriate for the description of biomass torrefaction kinetics. Di Blasi and Lanzetta [39] proposed a classical two-step kinetic model and obtained the corresponding kinetic parameters for xylan torrefaction. The classical kinetic model was generally accepted and widely used in the torrefaction kinetic modeling of biomass and its lignocellulosic components [33, 40-42]. Prins et al. [40] employed the Di Blasi – Lanzetta torrefaction model to describe the experimental torrefaction kinetic curves of willow (typical woody biomass)

at various temperatures (230 – 300 ℃) and obtained a different set of kinetic parameters. The model and those parameters were also used for the description of the torrefaction kinetics of other lignocellulosic biomass feedstocks (e.g., larch, willow and straw [43], and willow wood [44]). The summary of the above kinetic models for biomass torrefaction is shown in **Table 2**.

Table 2. Summary of kinetic models for biomass torrefaction in literature

Model	Characteristics	References
Empirical model	● Only statistical meaning ● Theoretical drawbacks ● For isothermal torrefaction	[35]
One-step model	● Not considering the competitive formation of volatile and solid products ● For isothermal torrefaction	[33, 36, 37]
Three-independent-parallel-reaction model	● Contradicting the torrefaction mechanisms ● For isothermal torrefaction	[38]
Two-step model	● Considering the competitive formation of volatile and solid products ● For isothermal torrefaction	[33, 38, 40-42]

Various kinetic models have been proposed to describe the kinetics of biomass torrefaction; however, most of them are only used to fit the mass loss experimental data of biomass during torrefaction. The evolution of torrefaction products (including torrefaction volatiles and solid products), the changes in compositions and energy contents of torrefaction products, and the effect of operation parameters (including heating rate, torrefaction temperature, torrefaction period) on biomass torrefaction are rarely found in relevant existed studies.

Although numerous studies on torrefaction kinetics of biomass have been reported, only a few of them have attempted to investigate the thermochemistry involved in the torrefaction process, which has an essential influence on the design of torrefaction system [45]. The results reported in the literature for the heat of torrefaction (the energy required to drive the torrefaction reactions) of woody biomass ranging from endothermic to large exothermic values [46, 47]. Some researchers directly suggested the heat of reaction for biomass torrefaction, but the details of the calculation were not given [27, 48].

In this study, poplar wood is used as a sample for biomass torrefaction. In literature, there existed several papers focusing on the torrefaction of poplar. Na et al. [49] investigated the changes in the chemical and physical properties of yellow poplar during torrefaction and concluded that hemicelluloses in poplar were affected by the

torrefaction temperature. According to Nhuchhen et al. [50], the net efficiency of poplar torrefaction in a continuous two-stage, indirectly heated rotary torrefaction reactor can reach above 88%. Kim et al. [51] investigated the physical and chemical characteristics of torrefied yellow poplar under different torrefaction conditions. They found that high temperature was appropriate for torrefaction to produce high energy density solid fuels. Silveria et al. [52] used the two-step kinetic model with different parameters from Prins et al. [40] to analyze the torrefaction kinetics of large scale poplar wood samples, and found that the kinetic parameters are sensitive to the torrefaction temperature range. However, the comprehensive study on the kinetics and thermochemistry of poplar torrefaction is still missing.

Therefore, the main objectives of this study are:

(1) to experimentally investigate and theoretically model the torrefaction kinetics of poplar wood under different torrefaction temperatures;

(2) the evolution kinetics of torrefaction products under different torrefaction conditions;

(3) to study the changes in elemental compositions and heating values of torrefaction volatiles and solid products;

(4) to perform the thermochemical analysis of poplar wood torrefaction focusing on the energy balance for poplar wood torrefaction in different conditions;

(5) to elucidate possible implications for the wood torrefaction industry.

This paper is organized as follows: Section 2 is the presentation of materials and experiments. Section 3 presents the kinetic and thermochemical models for biomass torrefaction and their numerical calculations. In Section 4, fitting of experimental data using torrefaction kinetic models, and the effect of temperature and heating rate on torrefaction, evolution kinetics of torrefaction volatiles and main elements during torrefaction and torrefaction thermochemistry of poplar wood are presented and discussed. Finally, some implications related on woody biomass torrefaction and conclusions of this work will be given in Section 5 and Section 6, respectively.

2 Materials and experiments
2.1 Materials

The biomass feedstock used in this study was poplar wood obtained from a farm located in Suqian City, Jiangsu Province, China. The samples underwent natural air-drying and were grinded into small particles with the particle sizes ranging from 0.18 to 0.25 mm for further physicochemical characterization and thermogravimetric analysis (TGA). Biomass is considered a poor heat conductor; therefore the small particle size of poplar wood (0.18 – 0.25 mm) and a heating rate of 20 ºC min^{-1} were used in order to reduce the non-uniform temperature in the samples during TGA [20]. Batch experiments of 10 g of biomass with particle sizes less than 2 mm accompanied by slow heating rates (less than 25 ºC min^{-1}) can ensure that the torrefaction is kinetically controlled according to Refs [24, 53]. The proximate analysis of the sample was performed in accordance with the ASTM standards (e.g., ASTM E871-82, ASTM

D1102-84, ASTM E872-82 for the determination of moisture, ash and volatile matter contents, respectively [54]). The sample was dried in a drying oven at 103 °C for 16 h to obtain the moisture content, then was heated in a muffle furnace at 590 °C for 4 h to determine the ash content. The sample was put in a corundum crucible with a closely fitting cover to measure the volatile matter content and then was heated at 950 °C for 7 min [54]. The ultimate analysis of the samples was measured in an elemental analyzer (Vario EL Cube Elemental Analyzer). The compositional analysis of the samples for the determination of the structural carbohydrates (including glucose, xylose, galcatose, arabinose and mannose) and lignin contents was performed in accordance with the National Renewable Energy Laboratory Standard Procedure (NREL/TP-510-42618) [55]. The analytical procedures are summarized as follows: (1) Pre-treated poplar wood particles were hydrolyzed by sulfuric acid and diluted by deionized water to get hydrolyzed liquid; (2) the liquid samples were detected by High Performance Liquid Chromatography (HPLC, Water 1515-2414) to obtain the content of structural carbohydrates, and UV-Visible spectrophotometer (UV-1800) to obtain the content of acid-insoluble lignin; (3) the acid-insoluble residue was heated at 105 and 575 °C, respectively, to determine the content of acid-insoluble lignin. In general, glucose is primarily derived from the depolymerization of cellulose and partially from hemicellulose, while xylose, galcatose, arabinose and mannose is from the depolymerization of hemicellulose [56].

A large number of correlations for higher heating values (HHVs) of solid fuels with their elemental compositions have been widely studied, reported and used in the literature [57-60]. The correlation from Channiwala and Parikh [61], which is one of the most widely used correlations for HHV predictions of solid fuels according to Scopus for its accuracy, has been used in this work for the estimation of the feedstock and torrefaction solid products' HHVs:

$$HHV = 34.91EC + 117.83EH + 10.05ES - 10.34EO - 1.51EN - 2.11Ash \qquad (1)$$

where HHV is the higher heating value (MJ kg^{-1}), EC, EH, ES, EO, EN and Ash are the elemental contents of C, H, S, O, N, and Ash on dry basis (kg kg^{-1}), respectively.

2.2 Experiments

TGA is a thermal analysis technique that monitors and records the change in sample mass against time or temperature in a controlled environmental furnace and can provide some information about some physical transitions and/or chemical reactions [62]. It is usually used for the kinetic measurement of thermal decomposition characteristics of biomass, coal and polymer [63]. The TGA of the poplar wood sample was performed in a thermogravimetric analyzer (TGA 7, Perkin Elmer, Inc., USA) in an inert atmosphere. Samples were dried at 105 °C for 12 hours to remove the moisture before the TGA test. In each experiment, about 4 – 5 mg of sample was used to reduce the impact of heat and mass transfer on the torrefaction kinetics. The sample was placed in a crucible, put on a balance inside the TGA furnace, and heated. Nitrogen (N$_2$) with high purity (>99.999%) was used as purge gas with a flow rate of 60 mL min^{-1} to ensure

the inert atmosphere during torrefaction. The TGA method used in this paper is according to the work from Prins [40]: the sample was heated from the initial temperature ($T_0 = 25\ ^{\circ}$C) to different final torrefaction temperatures ($T_f = 225, 250, 275$ and 300 $^{\circ}$C) with a heating rate of 20 $^{\circ}$C min^{-1}, and the final torrefaction temperature was kept constant for 60 min (residence time, t_r). The mass loss with time during torrefaction was recorded and analyzed. The mass loss data was normalized for further analysis.

3 Kinetic and thermochemical models for biomass torrefaction

3.1 Kinetic model and its numerical calculations

In this study, the classical two-step kinetic model proposed by Di Blasi and Lanzetta [39] and the kinetic parameter set obtained from Prins et al. [40] are employed to describe the torrefaction kinetic behaviors of poplar wood, since both have been widely used in kinetic analysis for the torrefaction of lignocellulosic biomass, especially for woody biomass. The torrefaction process of woody biomass is assumed as a series of sequential reactions: woody biomass (WB) decomposes into Volatile A (Va) and Solid Intermediate Products (SIP) through two parallel competing reactions, then SIP is assumed to further decompose into Volatile B (Vb) and torrefied biomass (TB) through two parallel competing reactions, as shown in **Figure 1**.
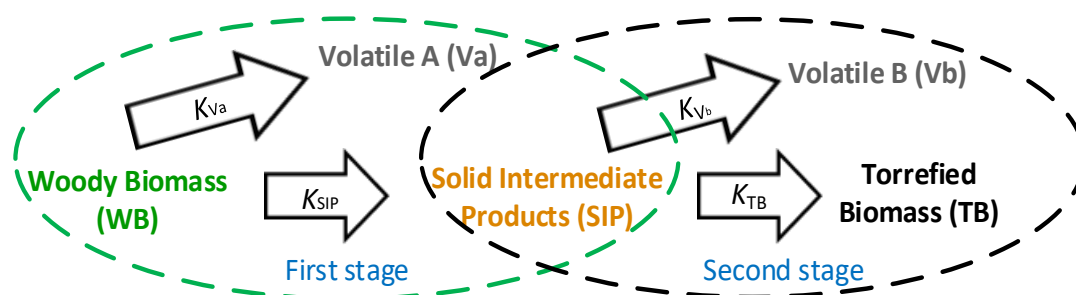

Figure 1. Reaction kinetic scheme of woody biomass torrefaction.

The corresponding kinetic equations for the torrefaction process presented in **Figure 1** can be obtained as follows:

$$\frac{dC_{WB}}{dt} = -\left(A_{Va}e^{-E_{Va}/RT} + A_{SIP}e^{-E_{SIP}/RT}\right)C_{WB} \tag{2}$$

$$\frac{dC_{Va}}{dt} = A_{Va}e^{-E_{Va}/RT}C_{WB} \tag{3}$$

$$\frac{dC_{SIP}}{dt} = A_{SIP}e^{-E_{SIP}/RT}C_{WB} - \left(A_{Vb}e^{-E_{Vb}/RT} + A_{TB}e^{-E_{TB}/RT}\right)C_{SIP} \tag{4}$$

$$\frac{dC_{Vb}}{dt} = A_{Vb}e^{-E_{Vb}/RT}C_{SIP} \tag{5}$$

$$\frac{dC_{TB}}{dt} = A_{TB}e^{-E_{TB}/RT}C_{SIP} \tag{6}$$

During torrefaction, the mechanisms of water evaporation and thermal decomposition

of biomass biopolymer components are different. Therefore, water evaporation will not be considered in the kinetic analysis of biomass torrefaction and the dry basis of the sample is concerned in further calculations and analysis. Considering that ash, N and S elements contained in woody biomass are unreactive, the initial conditions for the torrefaction process of woody biomass are simplified as:

$$
\begin{aligned}
C_{\text{WB}}\big|_{t=0} &= 100\% - C_{\text{Ash,WB}} - C_{\text{N,WB}} - C_{\text{S,WB}} \\
C_{\text{Va}}\big|_{t=0} &= 0 \\
C_{\text{SIP}}\big|_{t=0} &= 0 \\
C_{\text{Vb}}\big|_{t=0} &= 0 \\
C_{\text{TB}}\big|_{t=0} &= 0
\end{aligned}
\tag{7}
$$

where C (wt.%) represents the mass fraction of raw material and torrefaction products, the subscripts WB, SIP, TB, Va and Vb represent the values related to woody biomass, solid intermediate products, torrefied biomass, volatile A and volatile B, A (s^{-1}) is the frequency factor, E (kJ mol^{-1}) is the activation energy, t (s) is the time, T (K) is the temperature, $C_{\text{Ash,WB}}$ (wt.%), $C_{\text{N,WB}}$ (wt.%) and $C_{\text{S,WB}}$ (wt.%) are the mass fraction of ash, N and S in woody biomass, respectively. The values of the above kinetic parameters for woody biomass torrefaction are listed in **Table 3** [40].

Table 3. Kinetic parameters for woody biomass torrefaction [a]

Reaction	Parameter values	
	A (s^{-1})	E (kJ mol^{-1})
WB→Va	2.48×10^4	75.98
LB→SIP	3.23×10^7	114.21
SIP→Vb	1.10×10^{10}	151.71
SIP→TB	1.59×10^{10}	151.71

[a] Taken from Ref. [40] with permission of Elsevier.

The common heating programs used for studying the kinetics of biomass thermochemical conversion are the isothermal and linear heating programs [64]. In general, the raw material is torrefied from an initial temperature, T_0 (°C), at a heating rate, β (°C s^{-1}), to achieve the desired final torrefaction temperature, T_f (°C), which is kept constant for a set time. These temperature profiles are described using the following torrefaction kinetic model:

$$
T = \begin{cases} T_0 + \beta t & t \le \left(T_f - T_0\right)/\beta \\ T_f & t > \left(T_f - T_0\right)/\beta \end{cases}
\tag{8}
$$

As it is difficult to obtain the exact analytical solution for the above torrefaction kinetic model, numerical calculations are employed in this work. The classical fourth-

order Runge-Kutta method is an effective method for the numerical solution of the torrefaction kinetic model, which is based on Taylor formula and uses weighted mean to the integral slope with four points in integral interval [65]. **Figure 2** presents the flow diagram and pseudo-codes for the numerical calculations of the torrefaction kinetic model. The implementation of the numerical calculations was carried out in the MATLAB software system [66].
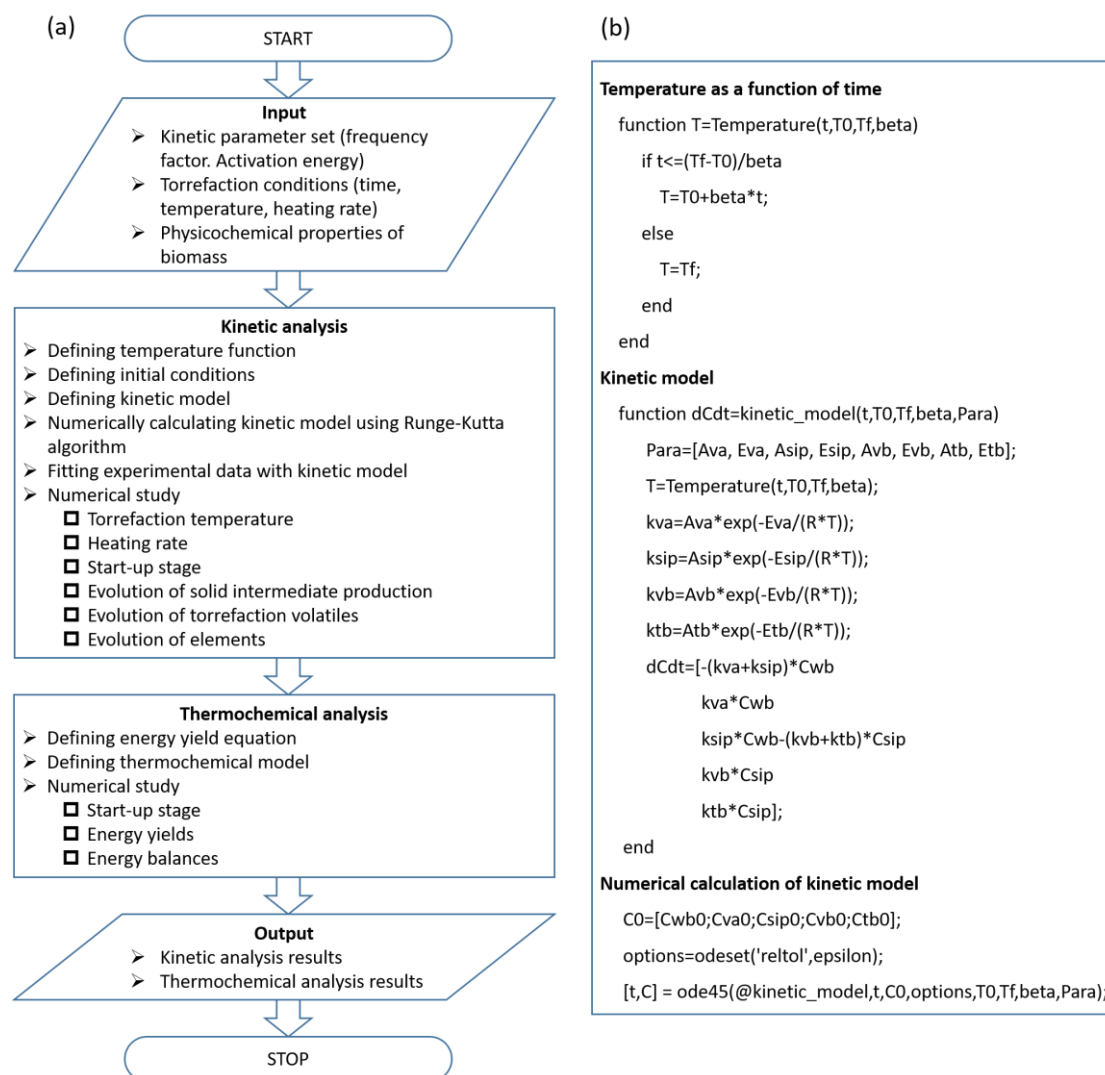

Figure 2. (a) Flow diagram and (b) pseudo-codes for numerical calculations of torrefaction kinetic model.

3.2 Thermochemical model and its calculations

The torrefaction of woody biomass has been characterized by the decomposition of hemicellulose and partial decomposition of cellulose during the first stage followed by the gradual degradation of the remaining cellulose in the second stage [67-69]. The contents of cellulose and hemicellulose vary little in quantity for most woody biomasses; on average, woody biomass contains 40 – 45 wt.% cellulose, 25 – 30 wt.% hemicellulose and 20 – 30 wt.% lignin [54, 56, 70]. Although, some differences exist

in the structures of hemicelluloses in woody biomass, the product yields and compositions of torrefaction products from different hemicelluloses during torrefaction are closely related [71]. Prins [72] found that the volatiles from willow torrefaction primarily included water, acetic acid, formic acid, methanol, lactic acid, furfural, hydroxy acetone, carbon dioxide and carbon monoxide and reported their average compositions at different process conditions. According to Chen et al. [68], during lignocellulosic biomass torrefaction, water is one of the most important products of two coupled reactions (oxygen removal and carbon migration), which transform the oxygen and/or carbon of lignocellulosic components into torrefaction liquid and gaseous products. Bates and Ghoniem [44] developed a simplified volatile composition model and predicted the chemical compositions of the pseudo-components Va and Vb (**Figure 1**). Some researchers [13, 44, 47, 72] measured the distribution of torrefaction volatiles from different woody biomasses, and the results indicated that the quantity and distribution of torrefaction volatiles were similar, which were also used in this study. **Table 4** lists these components as well as their physicochemical properties. Based on the chemical compositions and the mass contents of Va and Vb, their elemental compositions can be obtained and also listed in **Table 5**. The energy yields of the torrefaction solid residual , volatiles, and the enhancement factor of HHV can be calculated by Equations (9), (10) and (11), respectively.

$$\eta_{SR}(t) = \frac{C_{SR}(t) \cdot HHV_{SR}(t)}{HHV_{WB}} \times 100\% \tag{9}$$

$$\eta_{V}(t) = \frac{C_{Va}(t) \times HHV_{Va} + C_{Vb}(t) \times HHV_{Vb}}{HHV_{WB}} \times 100\% \tag{10}$$

$$EF_{SR}(t) = \frac{HHV_{SR}(t)}{HHV_{WB}} \tag{11}$$

where η_{SR} is the energy yield of the torrefaction solid residual, which is defined by the energy content ratio between the torrefaction solid residual and raw biomass; η_{V} is energy yield of the torrefaction volatiles, which is defined by the energy content ratio between the torrefaction volatiles and raw biomass; EF_{SR} is the enhancement factor, which can be defined as the HHV ratio between the torrefaction solid residual and raw biomass; C_{SR} is the mass fractions of main elements of the torrefaction solid residual, which can be determined by difference; HHV_{SR} is the heating value of the torrefaction solid residual which can be calculated by Equation (1) and HHV_{Va} and HHV_{Vb} are the heating value of torrefaction volatiles Va and Vb, respectively (see Table 4).

Table 4. Compositions of torrefaction volatiles and some physicochemical properties of volatile components

Chemical composition	Boiling point / °C	Latent heat of vaporization [a] / kJ kg⁻¹	Standard enthalpy of formation / kJ kg⁻¹	Mass content of Va / wt.%	Mass content of Vb / wt.%	HHV / kJ kg⁻¹	References
Water	100.02	2.455×10^3	-1.587×10^4	48.1	7.6	0	[73, 74]
Acetic acid	118.05	3.947×10^2	-8.052×10^3	14.8	16.1	1.457×10^4	[75, 76]
Formic acid	100.75	4.930×10^2	-9.236×10^3	5.3	5.1	5.514×10^3	[75, 77]
Methanol	64.65	1.099×10^3	-7.440×10^3	4.2	30.1	2.265×10^4	[75, 78]
Lactic acid	181.85	6.621×10^2	-6.894×10^3	1.3	31.3	1.371×10^4	[73, 79]
Furfural	161.55	5.266×10^2	-2.084×10^3	1.1	0.0	2.434×10^4	[79, 80]
Hydroxy acetone	145.55	5.670×10^2	-3.353×10^3	0.6	9.7	2.011×10^4	[81]
Carbon dioxide	-88.50	3.795×10^2	-8.941×10^3	20.4	0.0	0	[82]
Carbon monoxide	-191.52	2.142×10^2	-3.946×10^3	4.2	0.1	1.010×10^4	[82, 83]

Table 5. Elemental compositions and energy content of volatiles

	Volatile Va	Volatile Vb
Elemental compositions		
C	17.74 wt.%	36.34 wt.%
H	7.27 wt.%	8.78 wt.%
O	74.99 wt.%	54.88 wt.%
Energy content		
HHV	4.43×10^3 KJ kg⁻¹ [a]	1.633×10^4 KJ kg⁻¹ [a]

[a] Calculated by the HHVs and mass fractions of volatile components in volatiles Va and Vb

The estimation of the heat of reaction is essential for the establishment of energy balance of woody biomass torrefaction. To determine the heat of reaction for woody biomass torrefaction, the reaction pathways can be simplified as follow:

Woody biomass (WB) $\xrightarrow{\text{Torrefaction}}$ Volatiles (V) + Solid products (SP).

Based on the fundamental theory of thermodynamics, the heat of reaction for the torrefaction reaction process, ΔH_r (kJ kg⁻¹), can be calculated by the difference between the standard enthalpies of formation of the products and reactants[83]:

$$\Delta H_r(t) = \frac{C_{SP}(t)\cdot\Delta_f H_{SP}^{\Theta} + C_V(t)\cdot\Delta_f H_V^{\Theta} - \left[C_{WB}\big|_{t=0} - C_{WB}(t)\right]\cdot\Delta_f H_{WB}^{\Theta}}{C_{WB}\big|_{t=0} - C_{WB}(t)} \qquad (12)$$

where $\Delta_f H_{WB}^{\Theta}$, $\Delta_f H_{SP}^{\Theta}$, $\Delta_f H_V^{\Theta}$ (kJ kg⁻¹) are the standard enthalpies of formation of the raw material (woody biomass), solid products and volatiles from torrefaction, respectively, C_{WB}(dimensionless), C_{SP} (dimensionless) and C_V (dimensionless) are the mass fractions of the raw material (woody biomass), torrefaction solid products and

volatiles, respectively.

The raw material and torrefaction solid products are considered as non-conventional fuels. The standard enthalpy of formation of a non-conventional fuel ($C_xH_yO_zN_lS_m$) can be evaluated according to their elemental compositions and HHVs. To calculate the standard enthalpy of non-conventional fuels, the following combustion reaction is considered [84]:

$$C_xH_yO_zN_lS_m + \left(x + \frac{y}{4} + m - \frac{z}{2}\right)O_2 \rightarrow xCO_2 + \frac{y}{2}H_2O + \frac{l}{2}N_2 + mSO_2$$
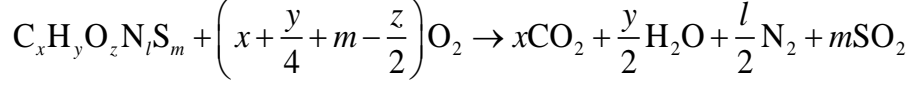
The enthalpy of formation for the above reaction satisfies the following expression:

$$(12x + y + 16z + 14l + 32m)\Delta_f H^\Theta_{C_xH_yO_zN_lS_m} = 44x \cdot \Delta_f H^\Theta_{CO_2} + 9y \cdot \Delta_f H^\Theta_{H_2O} + 14l \cdot \Delta_f H^\Theta_{N_2}$$

$$+ 64m \cdot \Delta_f H^\Theta_{SO_2} - 32\left(x + \frac{y}{4} + m - \frac{z}{2}\right)\Delta_f H^\Theta_{O_2}$$

$$+ (12x + y + 16z + 14l + 32m)HHV_{C_xH_yO_zN_lS_m}$$

$$(13)$$

where $\Delta_f H^\Theta_{C_xH_yO_zN_lS_m}$ (kJ kg^{-1}) is the standard enthalpy of formation of the non-conventional fuel ($C_xH_yO_zN_lS_m$) at the reference condition (25 °C and 1 atm), $\Delta_f H^\Theta_{CO_2}$,

$\Delta_f H^\Theta_{H_2O}$, $\Delta_f H^\Theta_{N_2}$, $\Delta_f H^\Theta_{SO_2}$, and $\Delta_f H^\Theta_{O_2}$ (kJ kg^{-1}) are the standard enthalpies of

formation of CO2, H2O, N2, SO2 and O2, respectively. $HHV_{C_xH_yO_zN_lS_m}$ (kJ kg^{-1}) is the

HHV of the non-conventional fuel. Since the standard enthalpy values of formation of N2 and O2 are zero, Equation (13) becomes:

$$\Delta_f H^\Theta_{C_xH_yO_zN_lS_m} = \frac{44x \cdot \Delta_f H^\Theta_{CO_2} + 9y \cdot \Delta_f H^\Theta_{H_2O} + 64m \cdot \Delta_f H^\Theta_{SO_2}}{12x + y + 16z + 14l + 32m} + HHV_{C_xH_yO_zN_lS_m} \quad (14)$$

The total enthalpy of formation of the unreacted biomass at the time t_m includes the standard enthalpy of formation and the sensible enthalpy required to the temperature T from T_0 of the unreacted raw material (Equation (15)).

$$\Delta_t H^\Theta_{WB}\Big|_{t=t_m} = m_0 \cdot \left[100 - C_{WB}(t_m) - C_{Ash,WB} - C_{N,WB} - C_{S,WB}\right] \cdot \Delta_f H^\Theta_{WB}$$

$$+ m_0 \cdot \int_{T_0}^{T|_{t=t_m}} \left[C_{WB}(t_m) + C_{Ash,WB} + C_{N,WB} + C_{S,WB}\right] \cdot c_{p,WB}(T)dT$$

$$(15)$$

where m_0 (kg) is the initial mass of the biomass and $c_{p,WB}$ (J kg^{-1} K^{-1}) is the specific

heat capacity of the raw material. The specific heat capacity of wood is dependent on various factors including the temperature and wood properties (e.g., particle size, moisture content, and the direction of the grain) [85]. In this work, the poplar wood samples were dried before thermogravimetric analysis for torrefaction kinetic

measurement and the samples used were well-ground particles whose particle size evenly distributed (particle diameters ranged from 0.18 – 0.25 mm), Therefore, the temperature-dependence specific heat capacity of the poplar wood sample is considered [86]:

$$c_{p,\mathrm{WB}}(T) = 1112.0 + 4.85T \tag{16}$$

where T is expressed in K and $c_{p,\mathrm{WB}}$ is expressed in J kg^{-1} K^{-1}.

The total enthalpy of formation of the torrefaction solid products at the time t_m includes the standard enthalpy of formation and the sensible enthalpy required to the temperature T from T_0 of the torrefaction solid products:

$$\begin{aligned}
\Delta_{\mathrm{t}} H_{\mathrm{SP}}^{\ominus}\big|_{t=t_m} = {} & m_0 \cdot \left[C_{\mathrm{SIP}}(t_m) + C_{\mathrm{TB}}(t_m) \right] \cdot \Delta_{\mathrm{f}} H_{\mathrm{SP}}^{\ominus} \\
& + m_0 \cdot \int_{T_0}^{T|_{t=t_m}} \left[C_{\mathrm{SIP}}(t_m) + C_{\mathrm{TB}}(t_m) \right] \cdot c_{p,\mathrm{SP}}(T)\,\mathrm{d}T
\end{aligned} \tag{17}$$

where $c_{p,\mathrm{SP}}$ (J kg^{-1} K^{-1}) is the specific heat capacity of the torrefaction solid products.

The properties of the torrefaction solid products are close to charcoal [27]. In this work, the formulae for the specific heat capacity of charcoal is used for the estimation of the specific heat capacity of the torrefaction solid products [87].

$$c_{p,\mathrm{SP}}(T) = 1003.2 + 2.09T \tag{18}$$

where T is expressed in K and $c_{p,\mathrm{SP}}$ is expressed in J kg^{-1} K^{-1}.

The standard enthalpy of formation of torrefaction volatiles, $\Delta_{\mathrm{f}} H_{\mathrm{V}}^{\ominus}$ (kJ kg^{-1}) can be estimated by the weighted sum of all torrefaction volatile components:

$$\Delta_{\mathrm{f}} H_{\mathrm{V}}^{\ominus} = \sum_{i=1}^{N_{\mathrm{V}}} \left(m_{\mathrm{V}_i} \cdot \Delta_{\mathrm{f}} H_{\mathrm{V}_i}^{\ominus} \right) \tag{19}$$

where N_{V} is the number of the components in the torrefaction volatiles, m_{V_i} (dimensionless) and $\Delta_{\mathrm{f}} H_{\mathrm{V}_i}^{\ominus}$ (kJ kg^{-1}) represent the relative mass content and standard enthalpy of formation of the ith component in the torrefaction volatiles, respectively.

The corresponding total enthalpy of formation of torrefaction volatiles is:

$$\Delta_{\mathrm{t}} H_{\mathrm{V}}^{\ominus}\big|_{t=t_m} = m_0 \cdot C_{\mathrm{V}}(t_m) \cdot \Delta_{\mathrm{f}} H_{\mathrm{V}}^{\ominus} + m_0 \cdot \sum_{i=1}^{N_{\mathrm{V}}} \int_{T_0}^{T|t=t_m} C_{\mathrm{V}_i}(T) \cdot c_{p,\mathrm{V}_i}(T)\,\mathrm{d}T \tag{20}$$

where c_{p,V_i} (J kg^{-1} K^{-1}) is the specific heat capacity of the ith component in the torrefaction volatiles (see Appendices), C_{V_i} is the mass fraction of the ith component

in the torrefaction volatiles and $C_V(t_m)$ is the mass fraction of the torrefaction volatiles at the time t_m.

4 Results and discussion
4.1 Physicochemical characteristics of poplar wood

The proximate, ultimate and compositional analysis results and HHV of the poplar wood sample are listed in **Table 6**.

Table 6. Physicochemical characteristics of poplar wood sample

Item	Poplar wood
Proximate analysis (on natural air-dried basis), wt.%	
Moisture	4.93±0.16
Ash	3.80±0.03
Volatile matter	73.07±0.14
Fixed carbon [a]	18.20
Ultimate analysis (on dry basis), wt.%	
C	42.77±0.09
H	6.12±0.04
O [a]	48.65
N	0.46±0.01
S	0.08±0.01
Energy content, (MJ kg^{-1})	
HHV [b]	17.07
Compositional analysis (on dry basis), wt.%	
Glucose	33.17±0.37
Xylose	12.75±0.58
Galcatose	1.99±0.03
Arabinose	0.09±0.00
Mannose	1.03±0.00
Acid-insoluble lignin	29.23±1.02
Acid-soluble lignin	2.30±0.06

[a] Obtained by difference; [b] Calculated by Equation (1).

4.2 Fitting of experimental data using torrefaction kinetic model

In torrefaction experiments, the measuring variable is the mass of solid residual, which is the sum of unreacted WB, SIP and TB. From Equations (2), (4) and (6), the change rate of the solid residual mass can be obtained:

$$\frac{dC_{SR}}{dt} = \frac{d}{dt}\left(C_{WB} + C_{SIP} + C_{TB}\right) = -\left(A_{Va}e^{-E_{Va}/RT}C_{WB} + A_{Vb}e^{-E_{Vb}/RT}C_{SIP}\right) \tag{21}$$

where C_{SR} (wt.%) is the mass fraction of the solid residual.

The mass fraction of the solid residual as a function of time can be obtained by the numerical integration of Equation (8) coupled with the initial conditions (7). It should be pointed out that the obtained C_{SR} *vs.* *t* data are on dry ash free basis.

The experimental data of poplar wood torrefaction and the data calculated by the classical one-step and two-step torrefaction kinetic models for poplar wood torrefaction kinetics at different torrefaction temperatures (225, 250, 275 and 300 ºC) are shown in **Figure 3**. The coefficients of determination, R^2, between the experimental data and the curves predicted from the model at different torrefaction temperatures are also included in **Figure 3**. R^2 is sometimes referred to as the "goodness of fit", which is a measure of how well the experimental data fits the model. It can be calculated by the equation: R^2=(TSS-RSS)/TSS (in the equation, RSS is the residual sum of squares, which is the sum of the squares of the experimental data minus the model prediction; TSS is the total sum of squares, which is the sum of the squares of the experimental data minus their mean). From the comparison illustrated in **Figure 3**, it can be obtained that (1) the classical two-step torrefaction kinetic model describes the kinetic experimental data of poplar wood torrefaction more accurate than the one-step model since the one-step model doesn't consider the competitive formation of torrefaction volatile and solid products; (2) all R^2 values are greater than 0.99 for the classical two-step torrefaction kinetic model, which indicates that the model is effective and accurate enough for the torrefaction kinetics of poplar wood at different torrefaction temperatures.
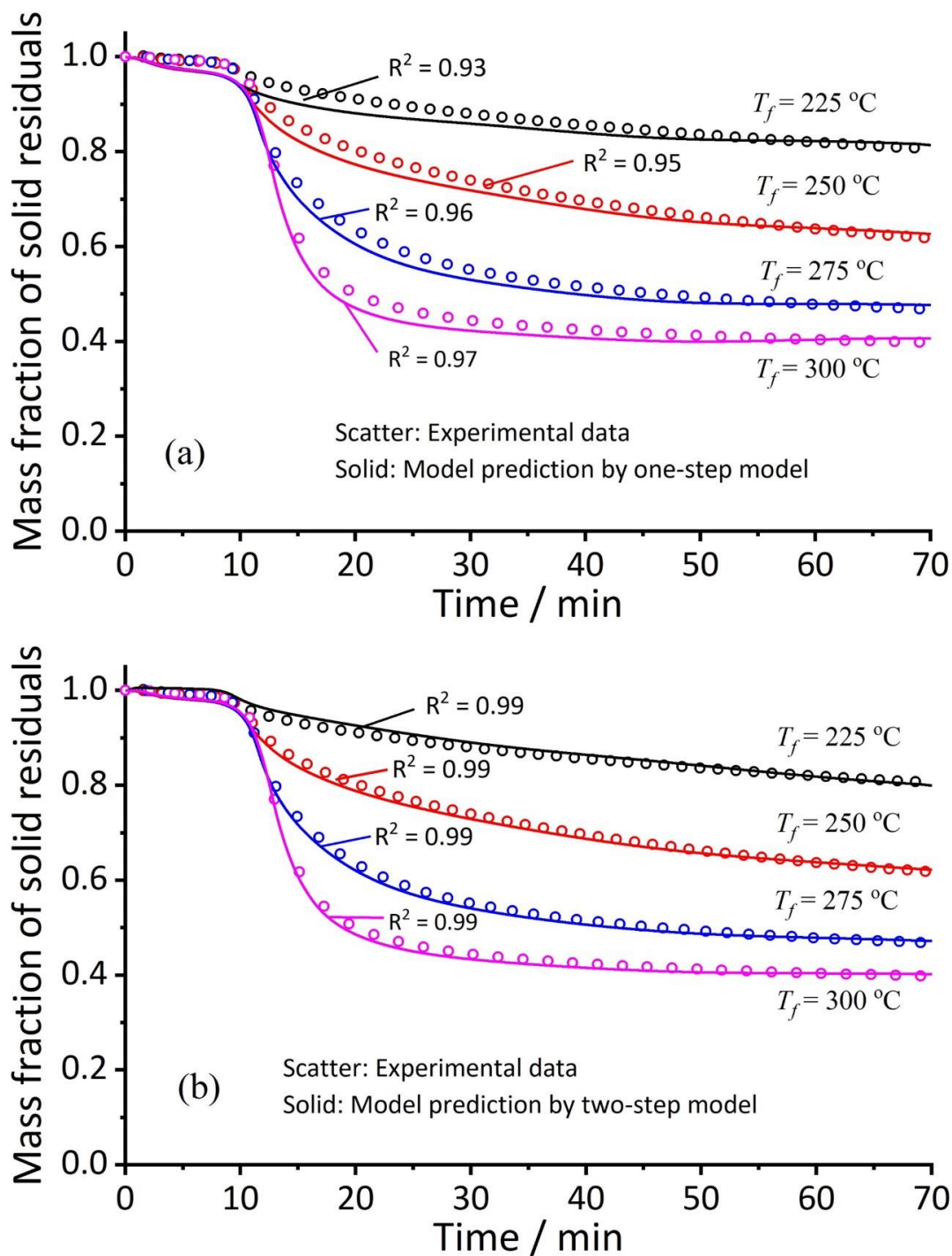
Figure 3. Comparison of experimental data and data predicted by (a) one-step and (b) two-step models for poplar wood torrefaction kinetics at various temperatures.

4.3 Effect of temperature and heating rate on torrefaction kinetics

The instantaneous fractional evolution and evolution rates of the raw material and torrefaction products numerically calculated from the torrefaction kinetic model at different torrefaction temperatures are shown in **Figure 4**. It presents that the evolution

of the raw material and torrefaction products is quicker at higher temperatures. At the initial stage of the torrefaction process, although the majority of the raw material (WB) converts into the intermediate products (SIP), it was observed that increasing amounts of Va were produced as the torrefaction temperature was increased. This indicates the important effect of temperature on the torrefaction product distribution, for example, higher temperatures facilitate a higher heating value and an increased product distribution towards more carbonaceous volatiles. From the kinetics point of view, the above conclusions are caused by the fact that the primary reaction has a lower activation energy than the secondary reaction in the torrefaction process. At low torrefaction temperature (e.g., 225 °C), the moisture and low molecular weight volatiles from the hemicellulose decomposition will be released, whereas cellulose and lignin are hardly decomposed [88-90]. When biomass undergoes torrefaction at high temperature (e.g., 275 and 300 °C), the thermal cracking reaction intensified and more volatiles were formed, in this scenario hemicellulose is almost decomposed completely whereas cellulose is partially degraded [23, 37]. Moreover, the decomposition of hemicellulose occurs through two stages: the cleavage of glycosidic bonds and the decomposition of side chains around 233 °C, followed by the fragmentation of monosaccharide units around 285 °C [68]. It was then observed that the increasing torrefaction temperature as the main factor for torrefaction not only increases the evolution rate of the torrefaction products, but also favors the formation of torrefaction volatiles (Va + Vb).
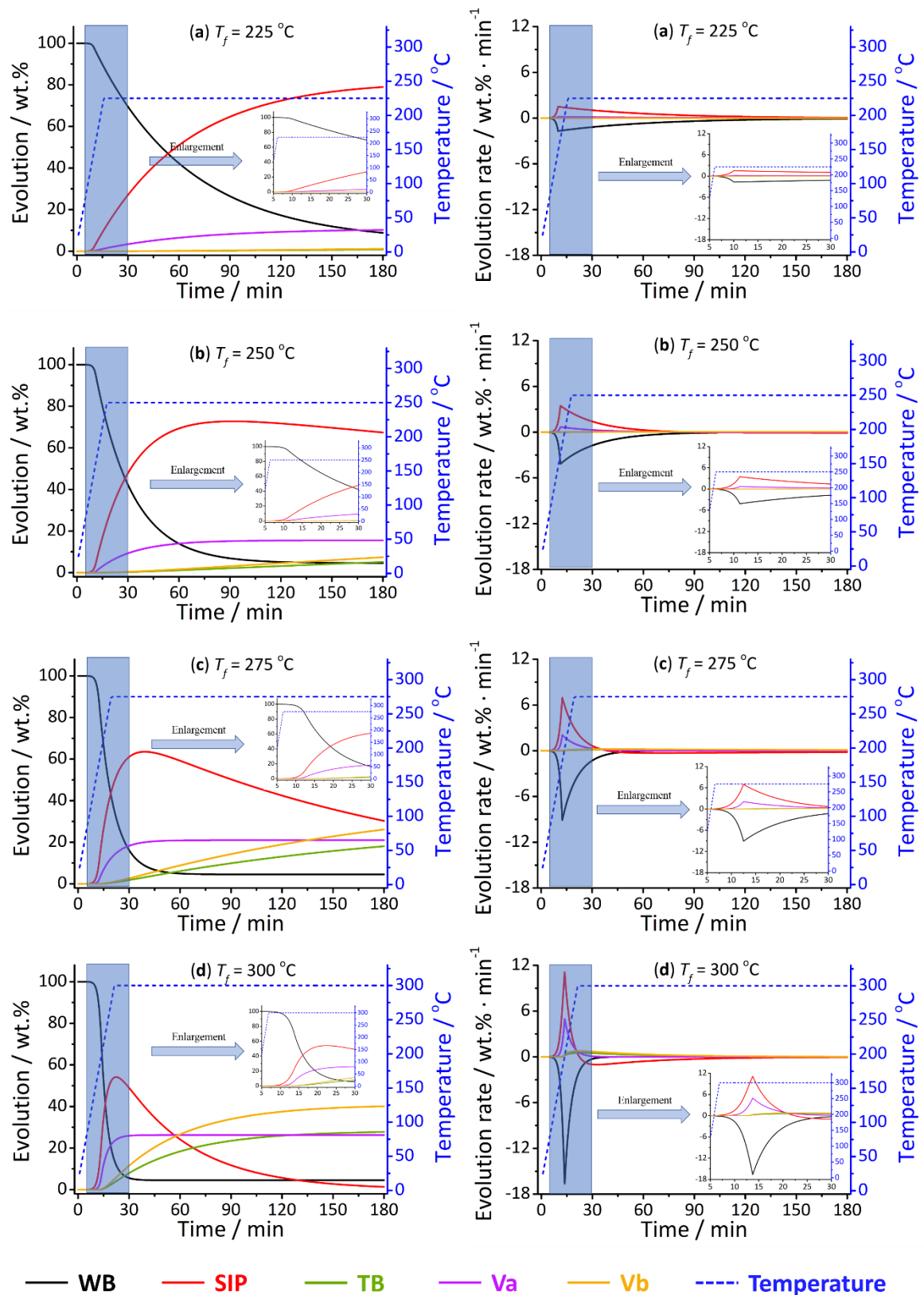
**Figure 4.** Evolution and evolution rate of poplar wood and torrefaction products during torrefaction at $T_0 = 25$ °C, $\beta = 20$ °C min^{-1}, and different torrefaction temperature: (a) $T_f = 225$ °C, (b) $T_f = 250$ °C, (c) $T_f = 275$ °C and (d) $T_f = 300$ °C. (The

results are obtained from the numerical calculations of the lignocellulosic biomass torrefaction kinetic model.)

The instantaneous fractional evolution and evolution rates of the raw material and torrefaction products at different heating rates and at a final torrefaction temperature of 275 °C are shown in **Figure 5**. From **Figure 5**, it can be obtained that as the heating rate was increased from 10 °C min^{-1} up to 40 °C min^{-1}, there was a shift of the evolution rate towards the left but also the evolution rates peaks for these components were sharpened, particularly for SIP and WB. Furthermore, the heating rate may also influence the final physicochemical characteristics of torrefied biomass according to the results reported by Supramono et al. [91]. They reported that the cellulose content of the torrefied sugarcane bagasse decreased from 10.61 wt.% to 5.35 wt.% with increasing of heating rate. They also reported that the increased lignin and hemicellulose contents, resulted in better hardness and stronger hydrophobicity.
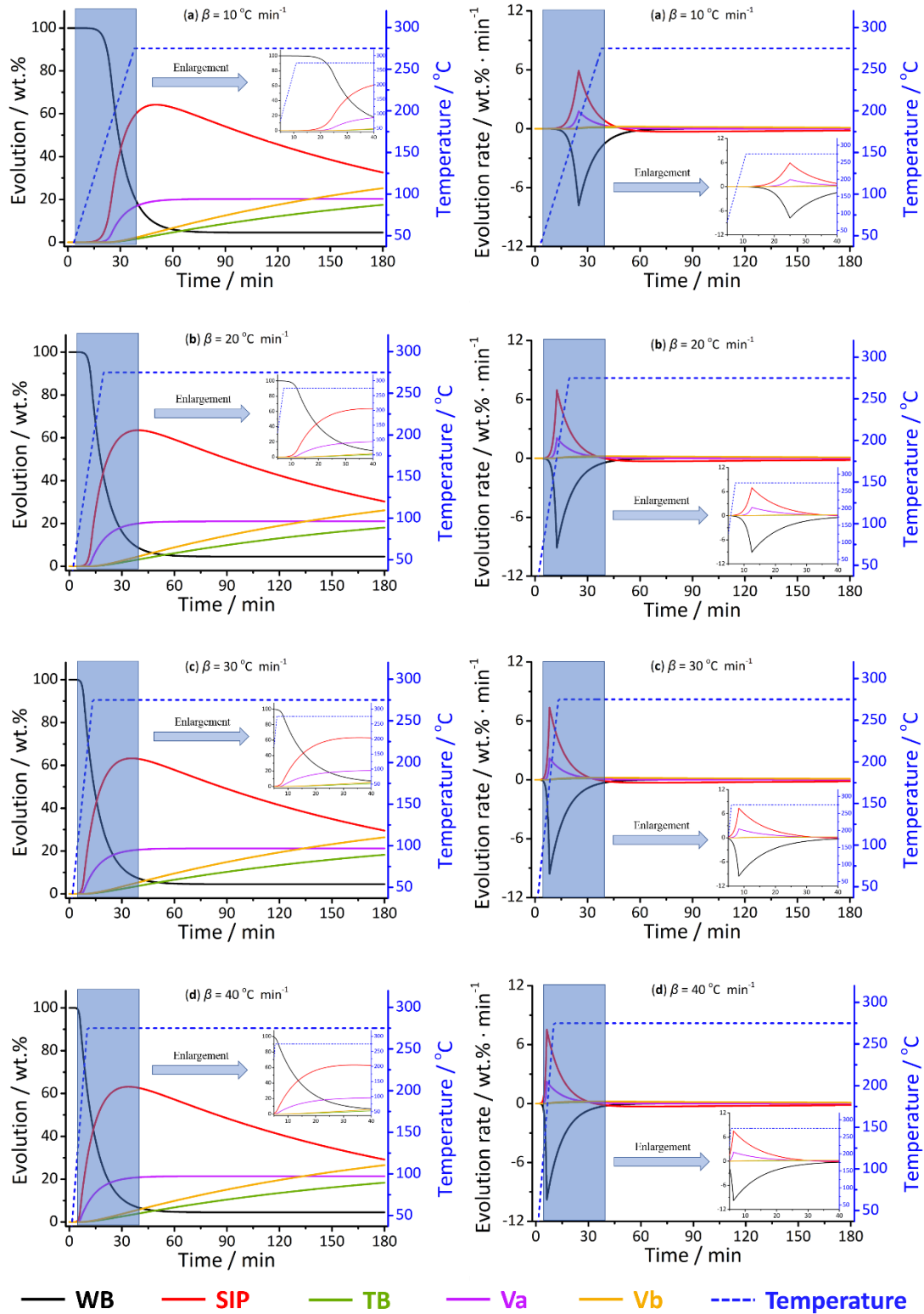
Figure 5. Evolution and evolution rate of poplar wood and torrefaction products during torrefaction starting at $T_0 = 25$ ºC, and up to $T_f = 275$ ºC and at different heating rates: (a) $\beta = 10$ ºC min^{-1}, (b) $\beta = 20$ ºC min^{-1}, (c) $\beta = 30$ ºC min^{-1} and (d) $\beta = 40$ ºC min^{-1}. (The results are obtained from the numerical calculations of the lignocellulosic biomass torrefaction kinetic model.)

Figure 5 shows that there is almost no mass loss occurring in the startup stage of the torrefaction process. To analyze the torrefaction startup stage quantitatively, the startup period (t_a) is defined between the starting time (e.g., $t = 0$ min) and the time when the mass loss of 0.1 wt.% for the raw material is reached (See **Figure 6(a)**).

The sensible heating energy (Q_a) and sensible heating power (P_a) in the torrefaction startup stage were calculated using the following equations:

$$Q_a = \int_{T_0}^{T_a} c_{p,\mathrm{WB}}(T)\mathrm{d}T \tag{22}$$

$$P_a = Q_a / t_a \tag{23}$$

where Q_a (kJ kg^{-1}) and P_a (kw kg^{-1}) are the startup sensible heating energy and power per unit mass, respectively, t_a (s) is the startup period, T_a (°C) is the startup torrefaction temperature (see **Figure 6(a)**), $c_{p,\mathrm{WB}}(T)$ is the specific heat capacity of the raw material (WB) which is dependent on temperature (described by Equation (16)).

The startup period, temperature, and sensible heating energy and power for the torrefaction of poplar wood at different heating rates (from 10 to 40 °C min^{-1}) were calculated using the aforementioned equations, and are depicted in **Figure 6(b)**. From **Figure 6(b)**, it can be observed that as the heating rate increases, the startup temperature as well as the sensible heating energy and power are increased, whereas the period of startup in minutes is reduced. This means that the time required for the startup period is reduced as more energy is provided to the system, and therefore increasing the energy transferred to the system resulting in increased sensible heating requirements.
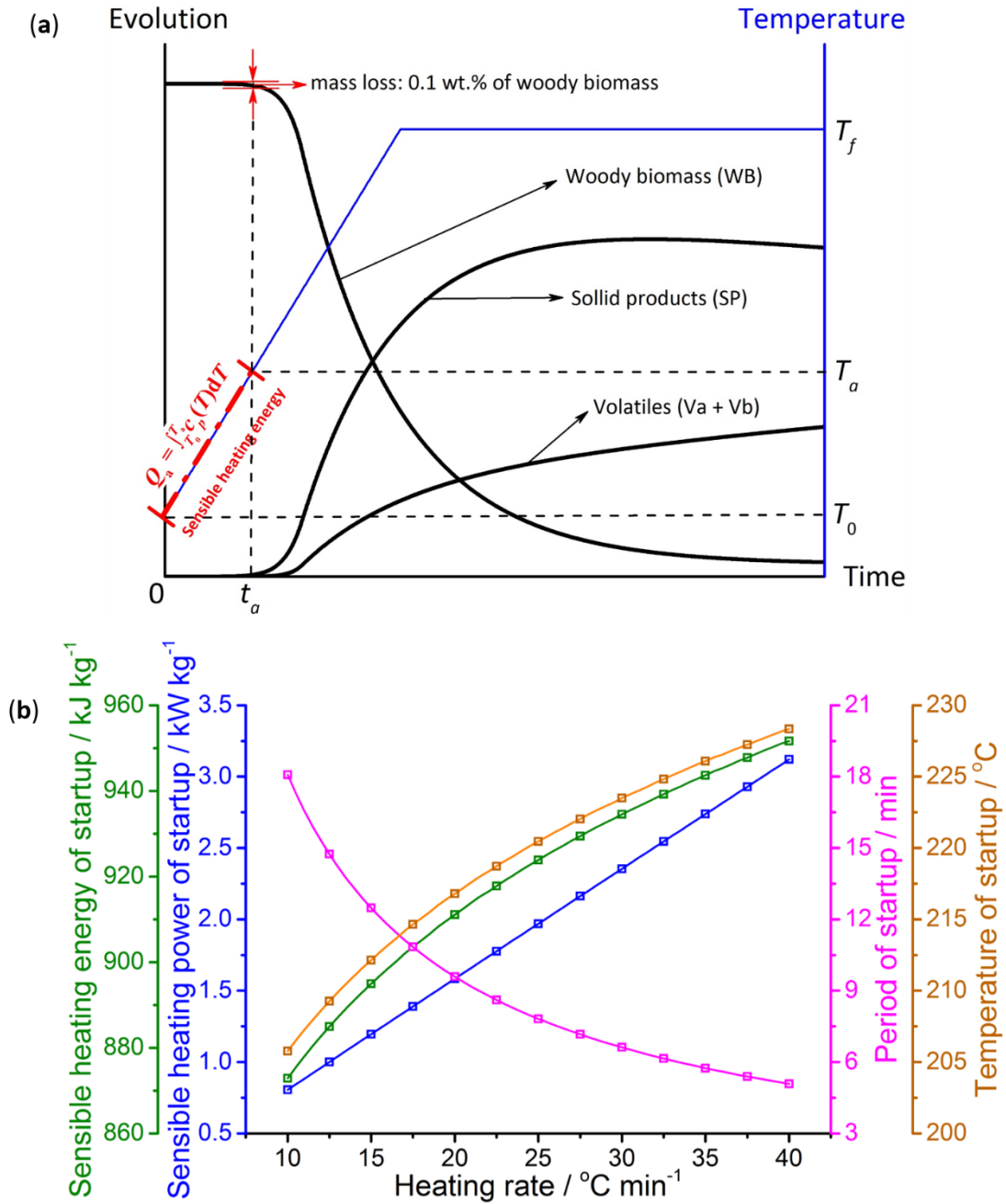
Figure 6. (a) Diagram of determination of start period, temperature, and sensible heating energy for poplar wood torrefaction; (b) Startup period, temperature, sensible heating energy and power for poplar wood torrefaction at $T_0 = 25$ °C, $T_f = 275$ °C and different heating rates (10 – 40 °C min^{-1}). (The results are obtained from the numerical calculations of the lignocellulosic biomass torrefaction kinetic model.)

Figure 7 illustrates the instantaneous fractional evolution of SIP and the time required to obtain the maximal yield of SIP during poplar wood torrefaction at different torrefaction temperatures (**Figure 7(a)**), and at different heating rates (**Figure 7(b)**). From **Figure 7**, it can be seen that the torrefaction temperature more significantly affects the evolution of SIP during torrefaction than the heating rate, and the time

required to obtain the maximum fraction of SIP decreases with increasing temperature. During torrefaction, higher final torrefaction temperature can facilitate the decomposition reaction in the first stage, thereafter can shorten the reaction time [40].
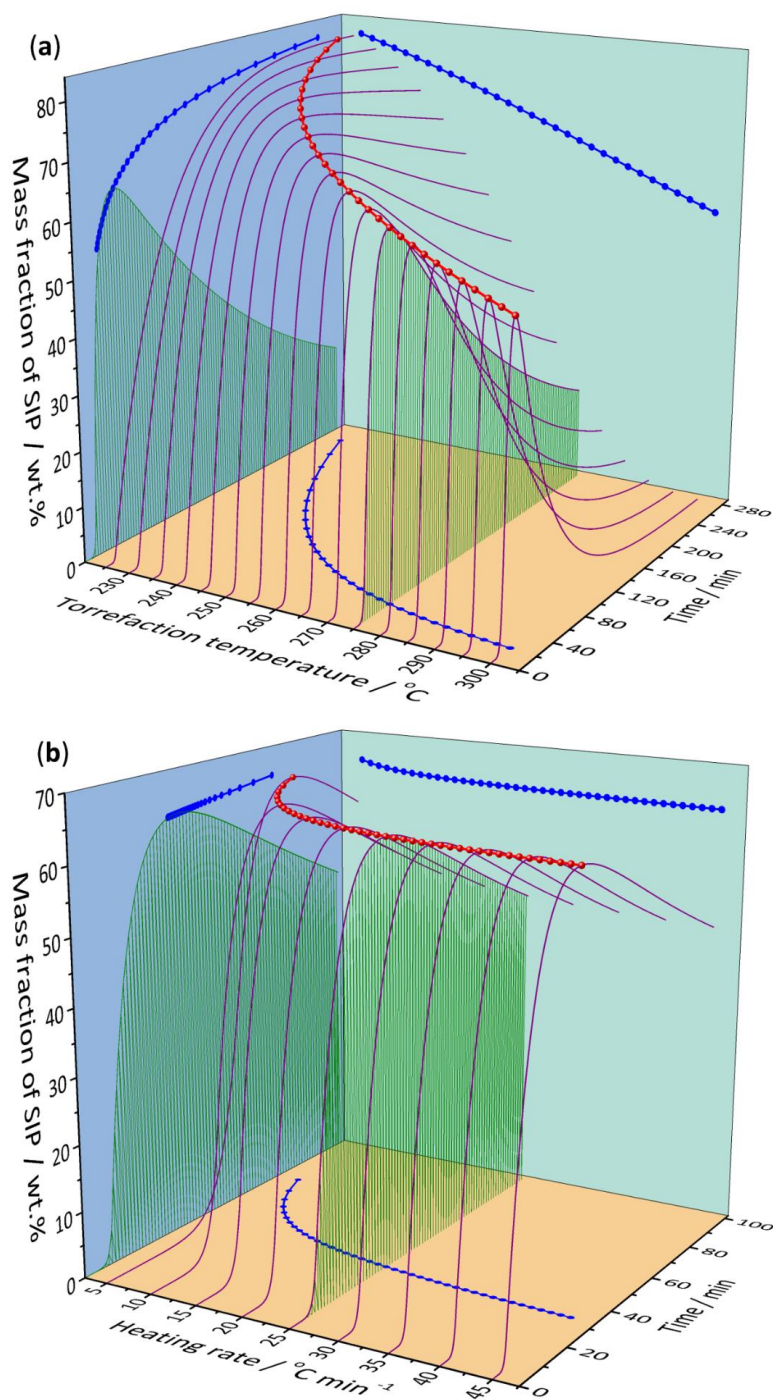
Figure 7. Evolution of SIP during poplar wood torrefaction at (a) $T_0 = 25$ °C, $\beta = 20$ °C min^{-1} and different T_f (225 – 300 °C) and (b) $T_0 = 25$ °C, $T_f = 275$ °C and different β (5 – 45 °C min^{-1}). (The results are obtained from the numerical calculations of the lignocellulosic biomass torrefaction kinetic model.)

4.4 Evolution of torrefaction volatiles

The evolution of overall torrefaction volatile reaction as well as volatile components with torrefaction time can be calculated using the following procedure: 1) the mass fractions of torrefaction volatiles Va and Vb at different torrefaction conditions can be obtained by the numerical integration of the classical two-step kinetic model for biomass torrefaction; 2) based on the relative contents of various torrefaction volatile components listed in Table 4 (data taken from Ref. [44]), the mass yields of individual volatile component in Va and Vb can be calculated, respectively; 3) simultaneously considering Va and Vb, the evolution and evolution rate of each torrefaction volatile component can be obtained. The corresponding results at the torrefaction temperatures of 250 °C and 275 °C are shown in **Figure 8**. It can be obtained that the overall yield of volatile components at 275 °C is almost twice as much as the yield at 250 °C. The higher yields of volatiles components such as acetic acid, furfural, methanol and formic acid at 275 °C are attributed to the decomposition products mainly from the side chains and substituents of hemicellulose [13], normally observed at a higher temperature [92]. The evolution rates of the volatile components obtained by the time derivative of the volatile yields are also shown in **Figure 8**. From **Figure 8**, it can be observed that the higher temperature can result in a quicker releasing rate of torrefaction volatiles.

Figure 9 shows the relative contents of the torrefaction volatiles at different final torrefaction temperatures (225 – 300 °C), and various residence times (60, 120, 180, and 240 min). Due to decarboxylation and dehydration reactions occurring during torrefaction, relatively high water and carbon dioxide contents appear in volatiles [47], and results in lower equilibrium moisture content and make torrefied biomass more hydrophobic [93]. With an increase of temperature, the relative contents of lactic acid and methanol significantly increase for all tested residence times. The cleavage of β-1,4-glycosidic bonds and the dehydration of hydroxyl are the major reactions occurring in cellulose torrefaction [94], while the cleavage of aryl ether linkages, demethoxylation, and dissociation of the aliphatic side chain are the major reactions for lignin torrefaction [95]. Hemicellulose shows poor thermostability in woody biomass contains acetoxy- and methoxy- groups attached to the polysugars (a particular xylose units), which can be decomposed to acetic acid and methanol especially at higher temperatures. The dehydration of hydroxyls and the dissociation of branches are the main reactions occurring in hemicellulose torrefaction at low temperature. Meanwhile, the fragmentation of monosaccharide residues is the main reactions at high temperature [96].
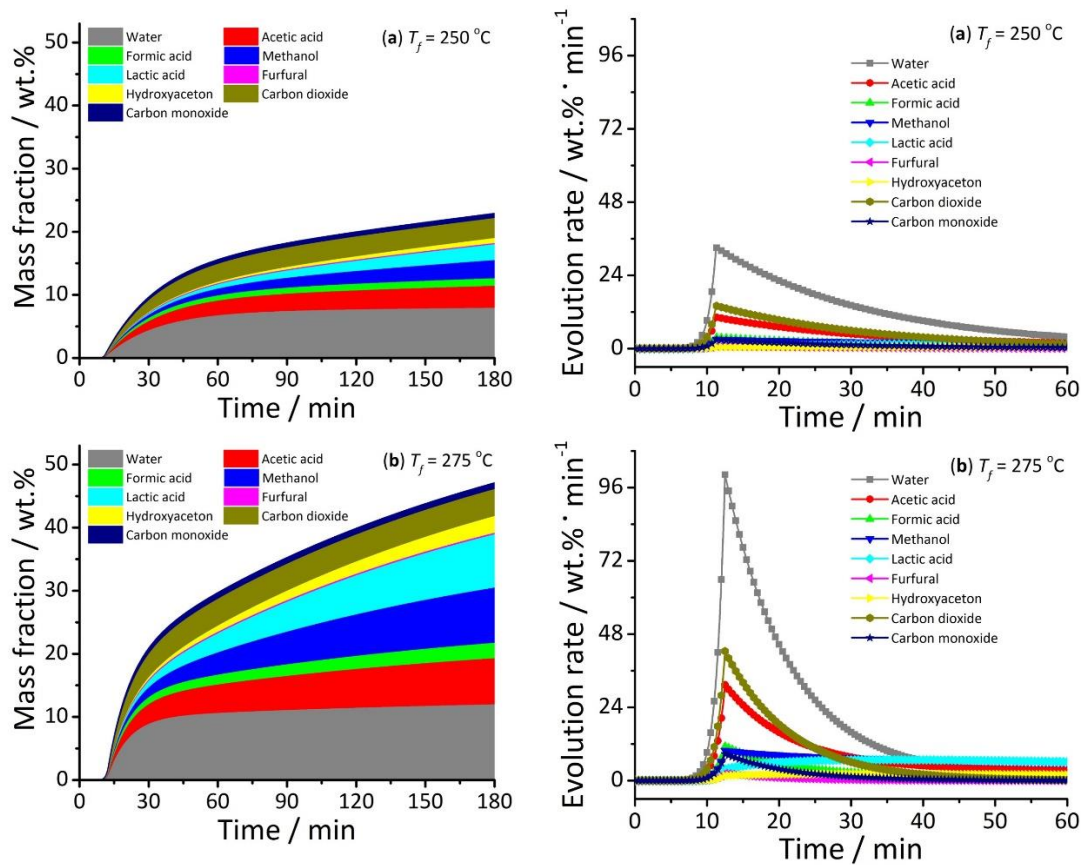
Figure 8. Evolution and evolution rate of torrefaction volatiles during poplar wood torrefaction at $T_0 = 25\ ^oC$, $\beta = 20\ ^oC\ min^{-1}$ and (a) $T_f = 250\ ^oC$ and (b) $T_f = 275\ ^oC$. (The results are obtained from the numerical calculations of the lignocellulosic biomass torrefaction kinetic model.)
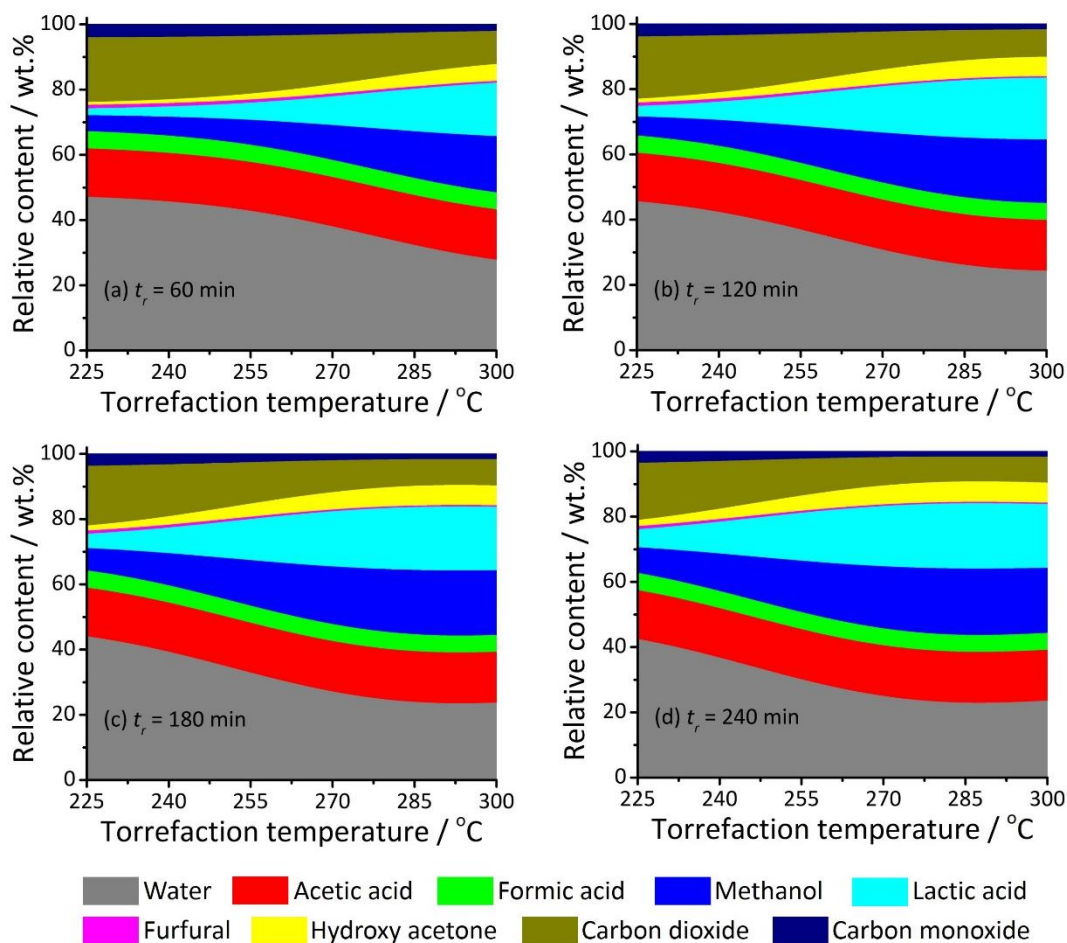
Figure 9. Relative contents of torrefaction volatile components during poplar wood torrefaction at $T_0 = 25$ °C, $\beta = 20$ °C min^{-1} and different temperatures (225 – 300 °C) with different torrefaction residence times (a) $t_r = 60$ min, (b) $t_r = 120$ min, (c) $t_r = 180$ min and (d) $t_r = 240$ min. (The results are obtained from the numerical calculations of the lignocellulosic biomass torrefaction kinetic model.)

4.5 Evolution of main elements during torrefaction

Figure 10 illustrates the evolution of main elements present in torrefaction solid residual and volatiles (**Figure 10(a)**), it also depicts the corresponding element ternary diagram of the torrefaction solid residual at different torrefaction periods (**Figure 10(b)**). For comparison, the results of some herbaceous biomass feedstocks [97] and coals with different ranks [98] were also included in **Figure 10**. The torrefaction solid residual loses much more Oxygen (O) than Carbon (C), and the corresponding evolution rate of O is much higher than that of C through the release of torrefaction volatiles, especially at the initial stage (0 – 30 min at $T_0 = 25$ °C, $\beta = 20$ °C min^{-1}, $T_f = 275$ °C). It might be caused by the decrease of aromatization and oxygenation and the intensified lignin content in the torrefaction solid residual[99]. In addition, the removed oxygen in torrefaction solid residual was transferred into the torrefied volatiles (e.g. CO_2, H_2O, CO, and acids) [16], and the removal of thermally unstable fragments during

28

torrefaction make the devolatilization change remarkably [100]. It was noted that the longer the torrefaction residence time, the elemental compositions of the torrefaction solid residual are closer than coal (a relatively high-quality solid fuel), these observations are in agreement with experimental data of wood briquette torrefaction obtained from Felfli et al. [99].
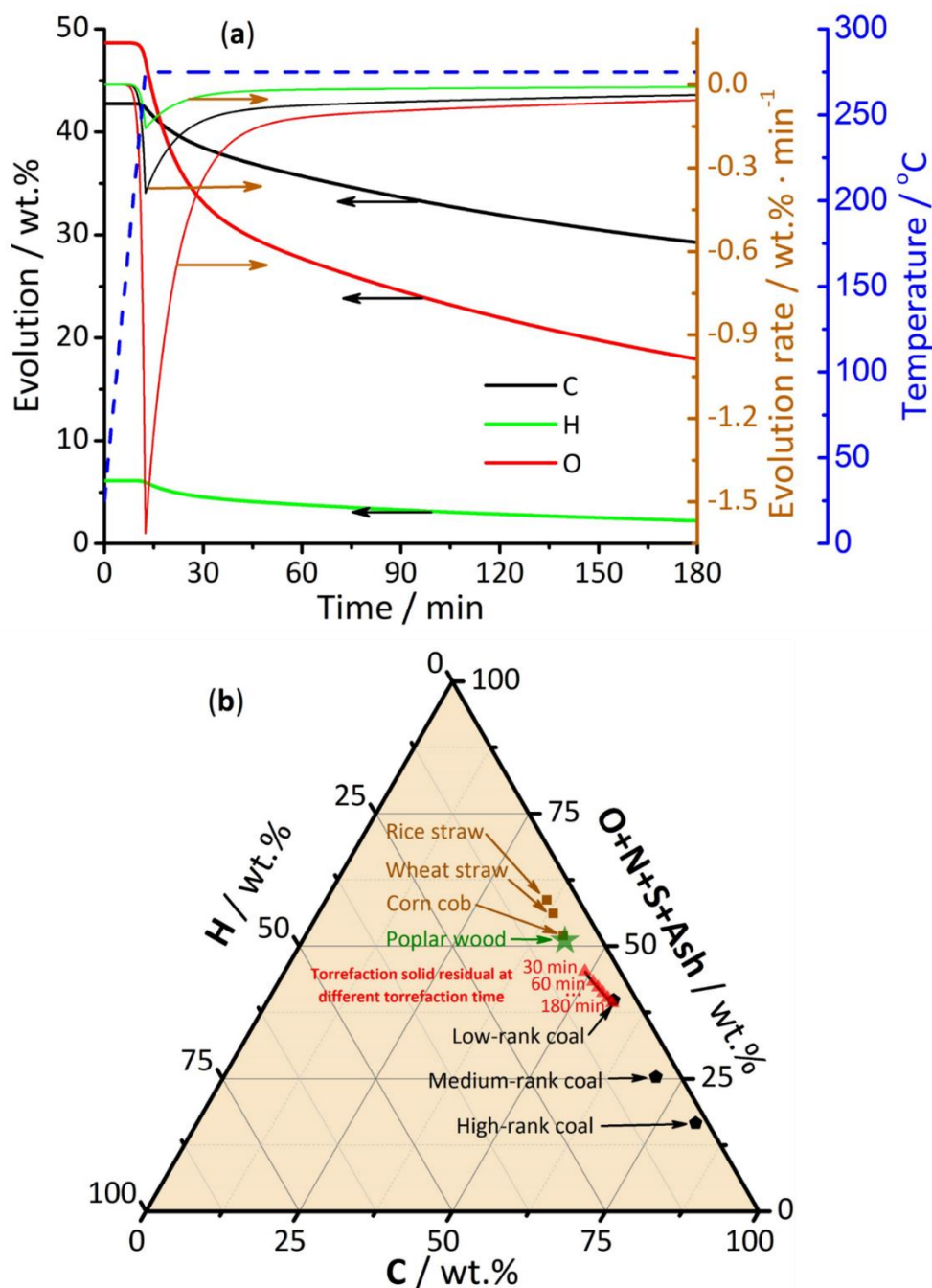

Figure 10. (a) Evolution and evolution rate of main elements in torrefaction solid residual during poplar wood torrefaction; (b) Element ternary diagram of poplar wood and torrefaction solid residual at $T_0 = 25$ °C, $\beta = 20$ °C min^{-1}, $T_f = 275$ °C and different torrefaction time (results of some herbaceous biomass feedstocks [97] and coals [98] are also included).

Figure 11 demonstrates the relative contents of C, H, O, N, S, Ash contained in the torrefaction solid residual at different torrefaction temperatures (225 – 300 $^{\circ}$C) and residence times (60, 120, 180, and 240 min). From **Figure 11**, it can be observed that for all the residence times, the torrefaction solid residual contains more C element and less O and H element at higher torrefaction temperature (270 – 300 $^{\circ}$C), which is in agreement with the trends reported by Adhikari et al. [101]. This phenomenon is mainly related to the decomposition temperature ranges of lignocellulosic components contained in woody biomass (hemicellulose: 250 – 350 $^{\circ}$C, cellulose 325 – 400 $^{\circ}$C and lignin: 300 – 550 $^{\circ}$C) [102].
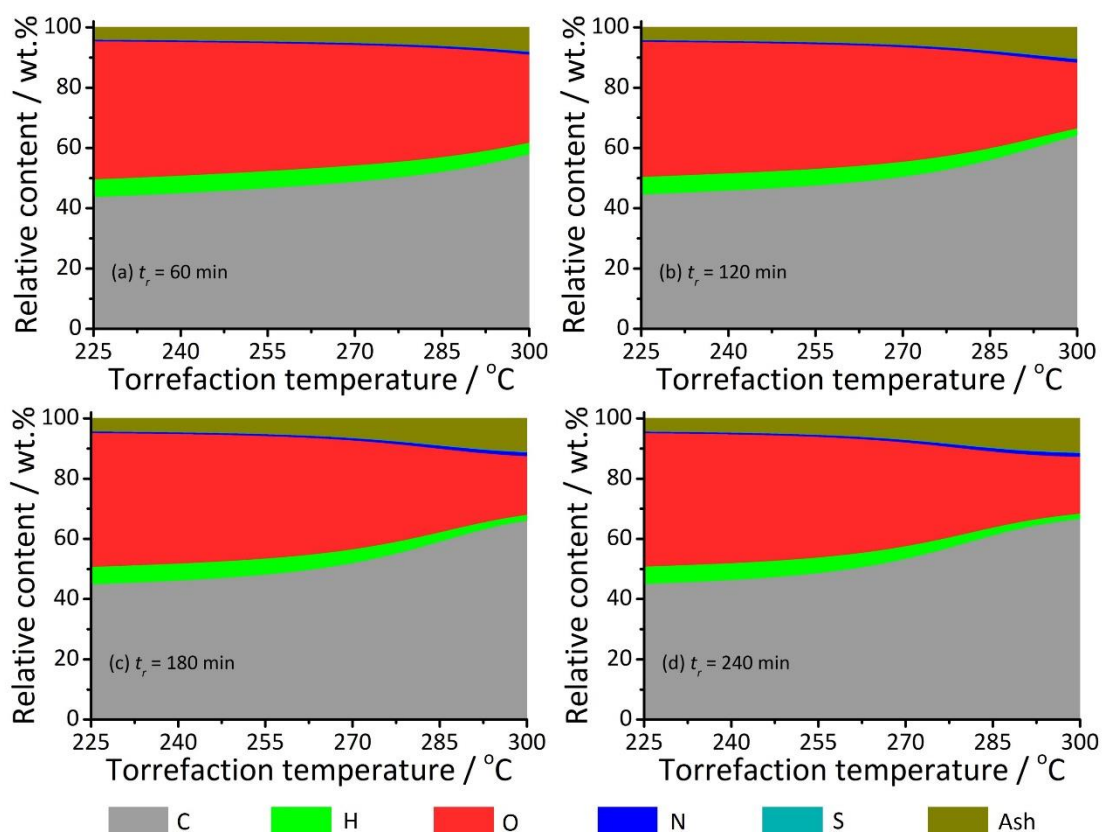

Figure 11. Relative contents of main elements and ash of torrefaction solid residual during poplar wood torrefaction at $T_0 = 25$ $^{\circ}$C, $\beta = 20$ $^{\circ}$C min^{-1} and different temperatures with different torrefaction residence time (a) $t_r= 60$ min, (b) $t_r= 120$ min, (c) $t_r= 180$ min and (d) $t_r= 240$ min. (The results are obtained from the numerical calculations of the lignocellulosic biomass torrefaction kinetic model.)

4.6 Energy yields of torrefaction products

Figure 12 illustrates the energy and mass yields of torrefaction solid residual and volatiles at $T_0 = 25$ $^{\circ}$C, $\beta = 20$ $^{\circ}$C min^{-1}, $T_f = 275$ $^{\circ}$C and $T_f = 300$ $^{\circ}$C with different torrefaction residence times. The longer the torrefaction residence time, the lower mass and energy yields of solid residual, and the higher mass and energy yields of volatiles. The energy yields of torrefied solid products decrease linearly with an increasing mass

loss of torrefaction solid materials, similar to the study performed by Peng et al. [103]. The enhancement factor of the torrefaction solid residual ranges from 1.00 to 1.24 within the torrefaction residence times of 180 min. Although a relatively large amount of solid residual mass loss occurs during torrefaction, the energy yields of torrefaction solid residual are relatively high. This behavior can be related to the releasing of non-combustible volatiles including CO_2 and H_2O during torrefaction especially in the initial torrefaction stage.
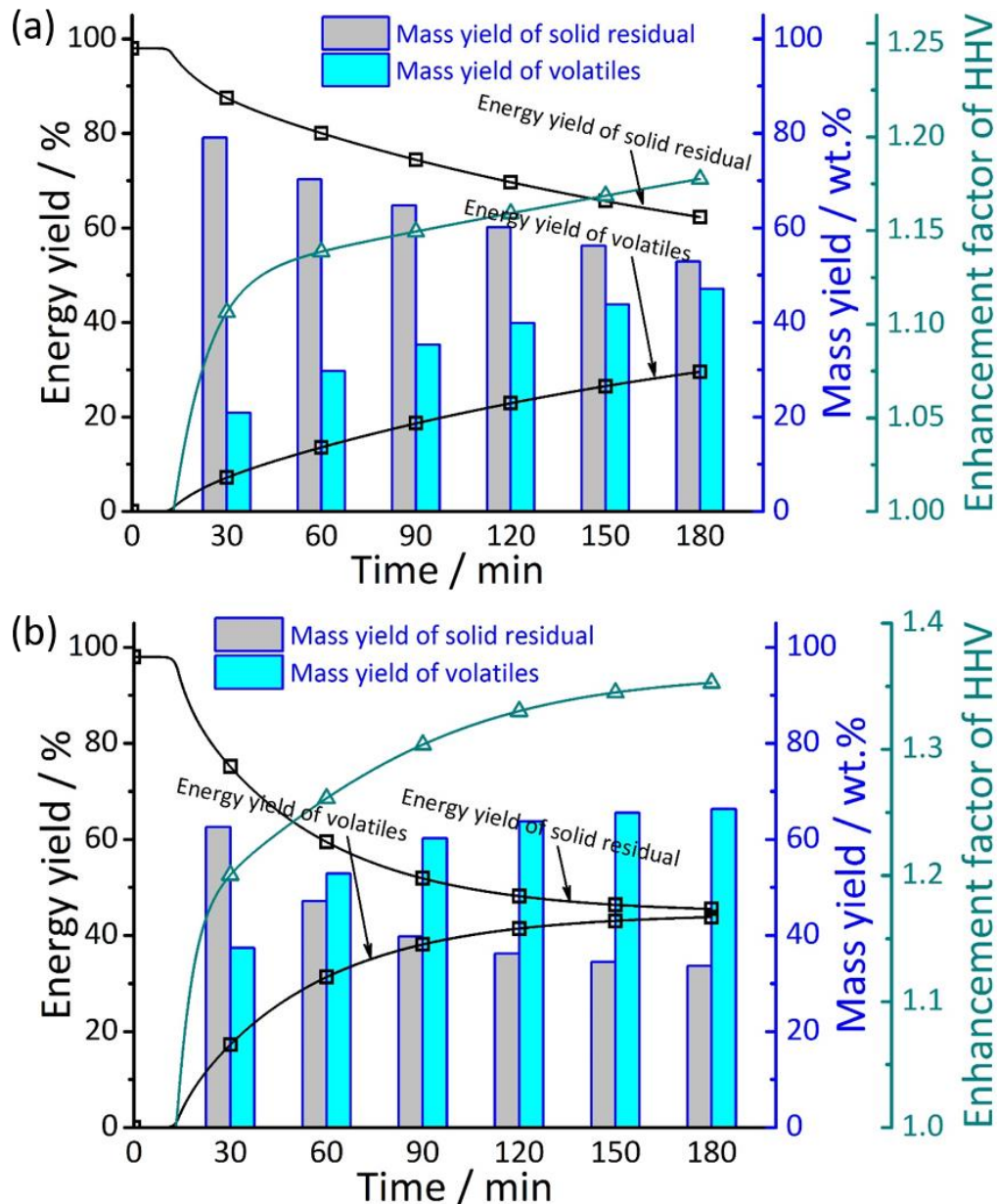
Figure 12. Energy and mass yields for poplar wood torrefaction at $T_0 = 25$ ºC, $\beta = 20$ ºC min^{-1}, and (a) $T_f = 275$ ºC and (b) $T_f = 300$ ºC with different torrefaction residence times. (The results are obtained from the numerical calculations of the lignocellulosic biomass torrefaction kinetic model.)

Figure 13 presents the energy and mass yields of torrefaction solid residual and volatiles at different torrefaction temperatures. The higher torrefaction temperature, the longer torrefaction residence time, the lower mass and energy yields of solid residual, and the higher mass and energy yields of volatiles. These observations suggest that torrefaction temperature has a much more significant impact than residence time on energy and mass yields. Furthermore, the influence from torrefaction temperature and residence time on energy yield is more violent than mass yield. Similar trends can be found in the torrefaction experimental data of pine chip and logging residue chip reported by Phanphanich et al. [104].
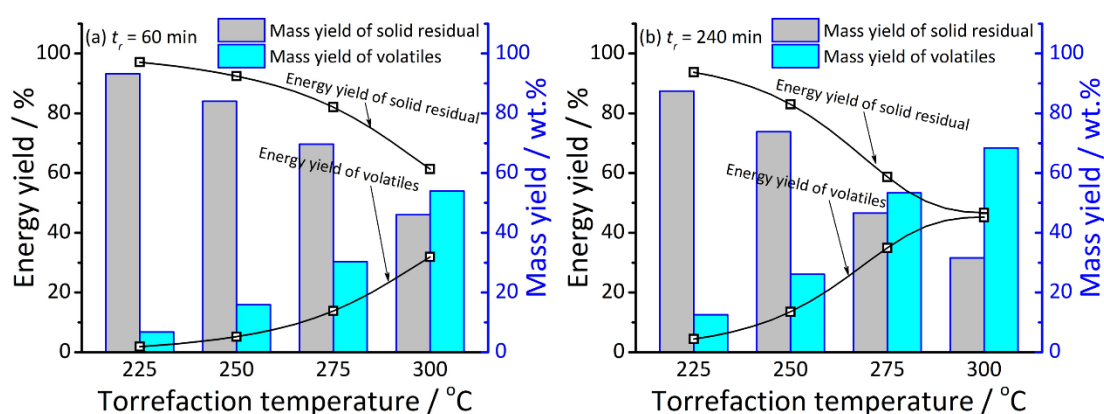

Figure 13. Energy and mass yields of torrefaction solid residual and volatiles during poplar wood torrefaction at $T_0 = 25$ °C, $\beta = 20$ °C min^{-1} and different torrefaction temperatures with different torrefaction residence times (a) $t_r = 60$ min and (b) $t_r = 240$ min. (The results are obtained from the numerical calculations of the lignocellulosic biomass torrefaction kinetic model.)

4.7 Thermochemical analysis of poplar woody torrefaction

There are several papers in the literature related to the mass and energy balances from the thermochemical analysis of woody biomass torrefaction [27, 48, 105]. Prins et al. [27] reported 87.2 wt.% mass yield and 96.6 % energy yield from the torrefaction of dry willow at 250 °C for 30 min, and 66.8 wt.% mass yield and 80.6 % energy yield at 300 °C for 10 min. The authors obtained the energy required for dry willow torrefaction from the reactor: 0.087 MJ kg^{-1} at 250 °C with 30 min and 0.124 MJ kg^{-1} at 300 °C with 10 min, respectively, which were calculated by difference between the energy contents of raw material and torrefaction products. In their study, the dependence of physicochemical properties of raw material and products on the temperature were not considered. Additionally they did not distinct between the heat of reaction for torrefaction and the energy requirement for heating up. Yan et al. [48] calculated the heat of reaction for loblolly pine torrefaction according to the thermodynamic theory: 0.25 MJ kg^{-1} at 260 °C with residence time of 5 min. However, the authors did not consider the sensible heat of raw material and products in their study,

which would lead to considerable system errors since the temperature of torrefaction products is much higher than room temperature. Besides, some over-simplified assumptions were made in the calculation of energy contents of torrefaction volatiles.

In this work, the energy balance for poplar wood torrefaction in different conditions has been calculated according to the thermochemical model presented in Section 3.2. The energy input for the torrefaction process of poplar wood included the energy content of raw material, energy for heating up and heat of torrefaction reaction; while the energy output included the energy content and sensible energy of torrefaction solid products, and energy content, sensible and latent energy of torrefaction volatiles. The heat of reaction for poplar wood torrefaction was determined by the difference between the standard enthalpies of formation of the products and reactants (Equation(12)). The energy for heating up of the raw material, the sensible and latent heat of torrefaction products were calculated according to the thermodynamic calculations presented in Section 3.2. In our calculations, the dependence of the properties of the raw material and torrefaction products on the temperature has been also considered.

Figure 14 presents the Sankey diagrams of poplar wood torrefaction at different torrefaction temperatures (225 – 300 ℃) with a torrefaction residence time of 60 min: the higher torrefaction temperature, the higher energy of heating up, the higher sensible and latent energy of volatiles, the higher energy content of volatiles and the lower energy content of solid products. The theoretical analysis results included in **Figure 14** indicate that the heat of torrefaction reaction is relatively small (which is about 10% of the energy content of the raw material) and it is also endothermic. The results are similar to those for torrefaction of loblolly pine reported by Yan et al. [48]. **Figure 14** also shows that as the torrefaction temperature was increased from 225 up to 275 ℃, the heat of torrefaction reaction also increased from 0.62 up to 1.67 MJ per kg of poplar wood; however, as the torrefaction temperature was further increased up to 300 ℃, the heat of torrefaction decreased to 1.46 MJ per kg of poplar wood. The variation of the sensible heat of solid products as function of the solid mass and temperature showed the same trend as that of the heat of torrefaction reaction with the temperature. For example, the sensible heat of solid products, as a function of mass and temperature, is just 0.22 MJ per kg of poplar wood even at 300 ℃ due to the low mass yield (41.87 wt.%) of torrefaction solid products. About 70% of the total energy input is transferred into torrefied biomass at 275 ℃ with torrefaction residence time of 60 min. Overall, it can be said that the sensible and latent energy of torrefaction products accounted for 5 – 18% of the total energy input, whereas the remaining energy input transferred into the energy contents of products in torrefaction process according to the results included in Table A2 in Appendices.
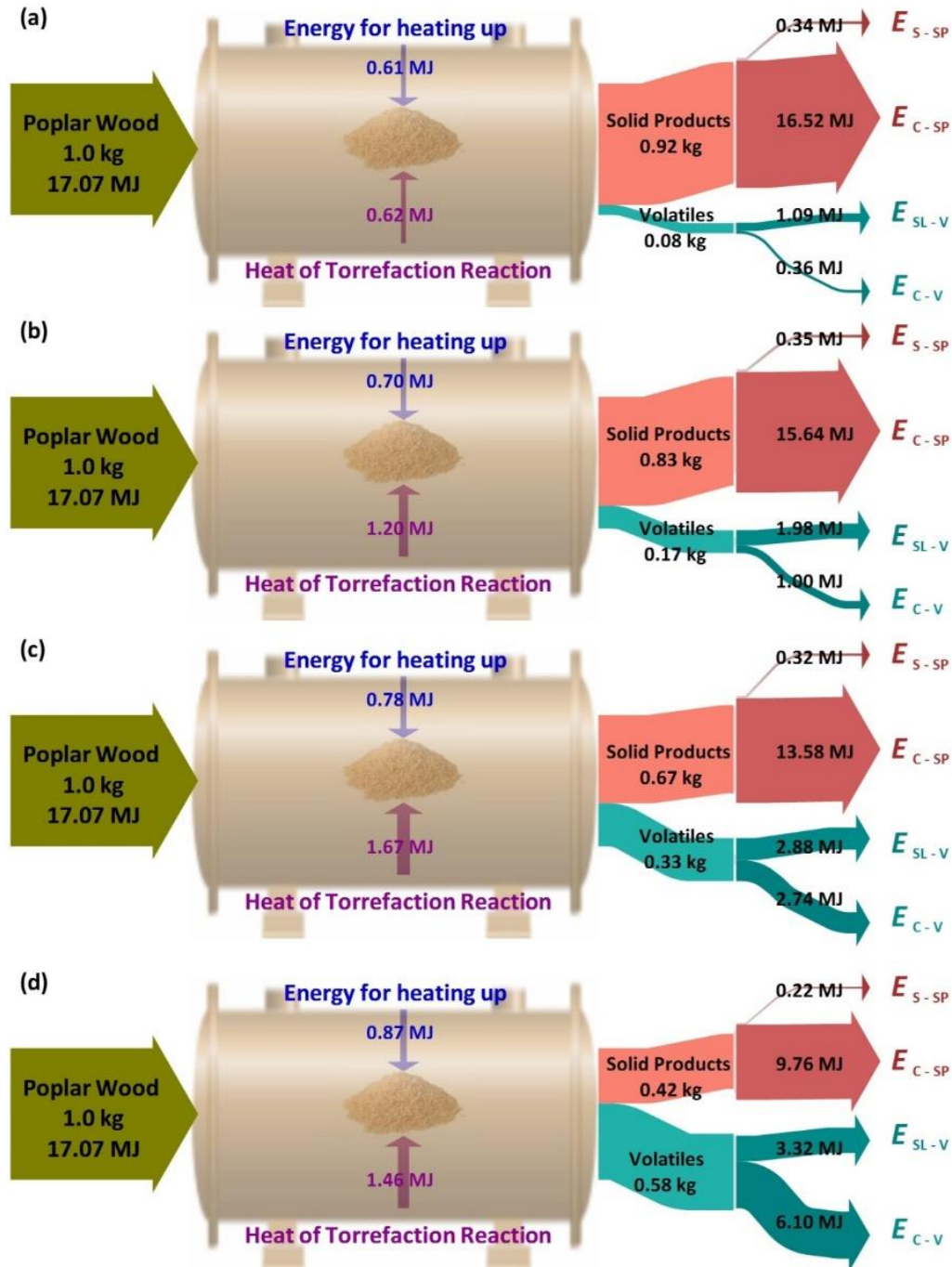
Figure 14. Sankey diagram of poplar wood torrefaction at $T_0 = 25\ ^{\circ}C$, $\beta = 20\ ^{\circ}C\ min^{-1}$, and (a) $T_f = 225\ ^{\circ}C$, (b) $T_f = 250\ ^{\circ}C$, (c) $T_f = 275\ ^{\circ}C$, (d) $T_f = 300\ ^{\circ}C$ with residence time of 60 min ($E_{S\text{-}SP}$, $E_{C\text{-}SP}$, $E_{SL\text{-}V}$, and $E_{C\text{-}V}$ represents sensible energy of solid products, energy content of solid products, sensible and latent energy of volatiles and energy content of volatiles, respectively).

5 Practical implications

According to the above study, the information of the kinetics of biomass torrefaction and the thermochemical performances of torrefaction processes are essential for the design, scale-up, optimization and industrial application of a biomass

torrefaction system. The flow chart of the overall design process of a biomass torrefaction system, from the initial proposal to the scale-up and industrial application, are shown in Figure 15. The kinetic and thermochemical models coupled with the specific model parameters can be used to establish the chemical models, which are coupled with the mass, momentum and energy conservation equations for the computation fluid dynamics simulation of torrefaction processes. Then the simulation results can be used for process optimization.
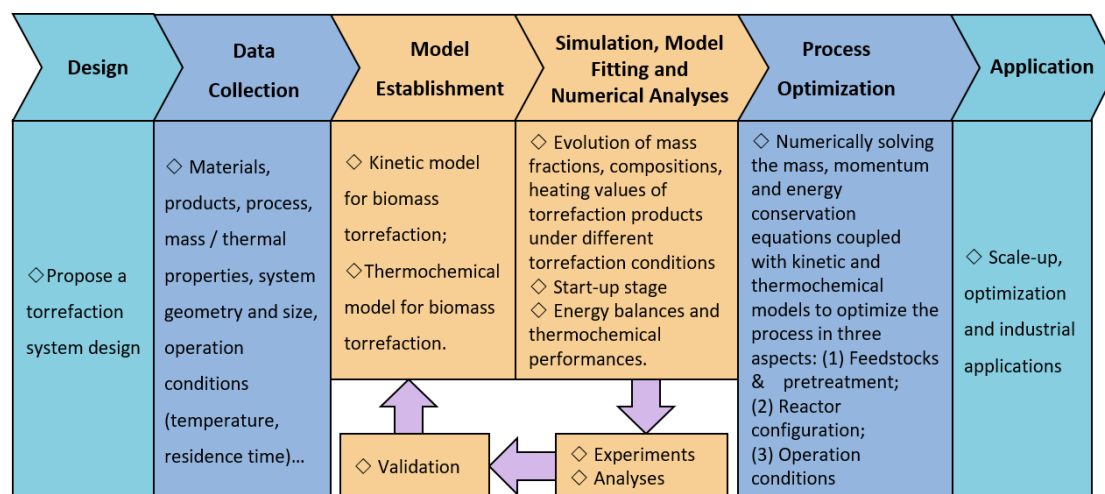

Figure 15. Flow chart for process design of biomass torrefaction system.

Torrefaction has gained attention in the bioenergy industry recently due to enhanced fuel properties (such as heating value, energy density, biological degradability) of torrefied biomass, which resemble those of coal. Although an energy input is required for the torrefaction process to proceed, torrefaction can enhance the fuel characteristics and thereafter reduce later costs associated with storage, transportation, and downstream processing of raw biomass. Additionally, if torrefied biomass is pelletized, the handing requirements, packing and transportation efficiencies are also improved due to their increased bulk density and good hydrophobicity [106].

The results obtained in this work in terms of evolution kinetic analysis of raw materials, torrefaction products and their elemental compositions, the start-up analysis of torrefaction, and the energy balance analysis, can provide theoretical guidance for the optimization of the torrefaction process parameters. This can be achieved according to the desired torrefaction distribution (mass yields of torrefaction products), torrefied biomass characteristics (energy density, densification, grindability, etc.) and process efficiency (e.g., heat loss and waste heat recovery).

6 Conclusions

1) Higher temperature (e.g., > 250 ℃) and longer residence time (e.g., > 30 min) facilitates the evolution of torrefaction, favors the formation of torrefaction volatiles, and accelerates aromatization and oxygenation reactions which lead to more carbon,

and less oxygen and hydrogen contents in the resulting torrefied biomass.

2) The heating rate has a slight effect on torrefaction evolution except at the heating up stage; the startup sensible heating power presents a linear relationship with the heating rate before 0.1 wt.% mass loss of poplar wood.

3) The torrefaction temperature has a more significant impact than residence time on mass and energy overall yields.

4) The heat of torrefaction reaction for poplar wood is endothermic and contributes with less than 10% of the energy content in the raw material. The sensible and latent energy of torrefaction products accounts for 5 - 18% of the total energy input and the remaining energy input transfers into energy contents of products.

5) The presented coupled kinetic and thermochemical model for poplar wood torrefaction can be helpful for the design, scale-up, optimization and industrial application of biomass torrefaction systems.

Acknowledgements

References

[1] Barskov S, Zappi M, Buchireddy P, Dufreche S, Guillory J, Gang D, et al. Torrefaction of biomass: A review of production methods for biocoal from cultured and waste lignocellulosic feedstocks. Renew Energ. 2019;142:624-42.

[2] Dai L, Wang Y, Liu Y, Ruan R, He C, Yu Z, et al. Integrated process of lignocellulosic biomass torrefaction and pyrolysis for upgrading bio-oil production: A state-of-the-art review. Renew Sust Energ Rev. 2019;107:20-36.

[3] Zhang J, Zhang X. 15 - The Thermochemical Conversion of Biomass into Biofuels. In: Verma D, Fortunati E, Jain S, Zhang X, editors. Biomass, Biopolymer-Based Materials, and Bioenergy: Woodhead Publishing; 2019. p. 327-68.

[4] Lin YC, Cho J, Tompsett GA, Westmoreland PR, Huber GW. Kinetics and mechanism of cellulose pyrolysis. J Phys Chem C. 2009;113:20097-107.

[5] Ma Z, Wang J, Zhou H, Zhang Y, Yang Y, Liu X, et al. Relationship of thermal degradation behavior and chemical structure of lignin isolated from palm kernel shell under different process severities. Fuel Process Technol. 2018;181:142-56.

[6] Huber GW, Iborra S, Corma A. Synthesis of transportation fuels from biomass: Chemistry, catalysts, and engineering. Chem Rev. 2006;106:4044-98.

[7] Kumar R, Strezov V, Weldekidan H, He J, Singh S, Kan T, et al. Lignocellulose biomass pyrolysis for bio-oil production: A review of biomass pre-treatment methods for production of drop-in fuels. Renewable and Sustainable Energy Reviews.

2020;123:109763.

[8] Wang S, Dai G, Yang H, Luo Z. Lignocellulosic biomass pyrolysis mechanism: A state-of-the-art review. Prog Energ Combust. 2017;62:33-86.

[9] Niu Y, Lv Y, Lei Y, Liu S, Liang Y, Wang D, et al. Biomass torrefaction: Properties, applications, challenges, and economy. Renew Sust Energ Rev. 2019;115:109395.

[10] Xin S, Huang F, Liu X, Mi T, Xu Q. Torrefaction of herbal medicine wastes: Characterization of the physicochemical properties and combustion behaviors. Bioresource Technol. 2019;287:121408.

[11] Xiao B, Sun XF, Sun R. Chemical, structural, and thermal characterizations of alkali-soluble lignins and hemicelluloses, and cellulose from maize stems, rye straw, and rice straw. Polym Degrad Stabil. 2001;74:307-19.

[12] Ru B, Wang S, Dai G, Zhang L. Effect of torrefaction on biomass physicochemical characteristics and the resulting pyrolysis behavior. Energy Fuel. 2015;29:5865-74.

[13] Prins MJ, Ptasinski KJ, Janssen FJJG. Torrefaction of wood : Part 2. Analysis of products. J Anal Appl Pyrol. 2006;77:35-40.

[14] Basu P, Sadhukhan AK, Gupta P, Rao S, Dhungana A, Acharya B. An experimental and theoretical investigation on torrefaction of a large wet wood particle. Bioresource Technol. 2014;159:215-22.

[15] Ma Z, Zhang Y, Shen Y, Wang J, Yang Y, Zhang W, et al. Oxygen migration characteristics during bamboo torrefaction process based on the properties of torrefied solid, gaseous, and liquid products. Biomass Bioenerg. 2019;128:105300.

[16] Ma Z, Wang J, Li C, Yang Y, Liu X, Zhao C, et al. New sight on the lignin torrefaction pretreatment: Relevance between the evolution of chemical structure and the properties of torrefied gaseous, liquid, and solid products. Bioresource Technol. 2019;288:121528.

[17] Zhang C, Ho S-H, Chen W-H, Xie Y, Liu Z, Chang J-S. Torrefaction performance and energy usage of biomass wastes and their correlations with torrefaction severity index. Appl Energ. 2018;220:598-604.

[18] Iroba KL, Baik O-D, Tabil LG. Torrefaction of biomass from municipal solid waste fractions II: Grindability characteristics, higher heating value, pelletability and moisture adsorption. Biomass Bioenerg. 2017;106:8-20.

[19] Sindhu R, Binod P, Pandey A. Biological pretreatment of lignocellulosic biomass – An overview. Bioresource Technol. 2016;199:76-82.

[20] Ohliger A, Förster M, Kneer R. Torrefaction of beechwood: A parametric study including heat of reaction and grindability. Fuel. 2013;104:607-13.

[21] Wang L, Barta-Rajnai E, Skreiberg Ø, Khalil R, Czégény Z, Jakab E, et al. Effect of torrefaction on physiochemical characteristics and grindability of stem wood, stump and bark. Appl Energ. 2018;227:137-48.

[22] Arias B, Pevida C, Fermoso J, Plaza MG, Rubiera F, Pis JJ. Influence of torrefaction on the grindability and reactivity of woody biomass. Fuel Process Technol. 2008;89:169-75.

[23] Chen WH, Cheng WY, Lu KM, Huang YP. An evaluation on improvement of

pulverized biomass property for solid fuel through torrefaction. Appl Energ. 2011;88:3636-44.

[24] Acharya B, Pradhan R, Dutta A. Qualitative and kinetic analysis of torrefaction of lignocellulosic biomass using DSC-TGA-FTIR. AIMS Energy. 2015;3:760-73.

[25] Ukaew S, Schoenborn J, Klemetsrud B, Shonnard DR. Effects of torrefaction temperature and acid pretreatment on the yield and quality of fast pyrolysis bio-oil from rice straw. J Anal Appl Pyrol. 2018;129:112-22.

[26] Bi D, Li B, Liu S, Yi W, Jiang M, Lin Z. Influence of Pyrolysis and Torrefaction Pretreatment Temperature on the Pyrolysis Product Distribution. BioRes. 2018;14:13.

[27] Prins MJ, Ptasinski KJ, Janssen FJJG. More efficient biomass gasification via torrefaction. Energy. 2006;31:3458-70.

[28] Brachi P, Chirone R, Miccio F, Miccio M, Ruoppolo G. Entrained-flow gasification of torrefied tomato peels: Combining torrefaction experiments with chemical equilibrium modeling for gasification. Fuel. 2018;220:744-53.

[29] Chew JJ, Soh M, Sunarso J, Yong S-T, Doshi V, Bhattacharya S. Gasification of torrefied oil palm biomass in a fixed-bed reactor: Effects of gasifying agents on product characteristics. J Energy Inst. 2020;93:711-22.

[30] Bridgeman TG, Jones JM, Shield I, Williams PT. Torrefaction of reed canary grass, wheat straw and willow to enhance solid fuel qualities and combustion properties. Fuel. 2008;87:844-56.

[31] Fisher EM, Dupont C, Darvell LI, Commandré JM, Saddawi A, Jones JM, et al. Combustion and gasification characteristics of chars from raw and torrefied biomass. Bioresource Technol. 2012;119:157-65.

[32] Panahi A, Vorobiev N, Schiemann M, Tarakcioglu M, Delichatsios M, Levendis YA. Combustion details of raw and torrefied biomass fuel particles with individually-observed size, shape and mass. Combust Flame. 2019;207:327-41.

[33] Shang L, Ahrenfeldt J, Holm JK, Barsberg S, Zhang R-z, Luo Y-h, et al. Intrinsic kinetics and devolatilization of wheat straw during torrefaction. J Anal Appl Pyrol. 2013;100:145-52.

[34] Bach Q-V, Chen W-H, Eng CF, Wang C-W, Liang K-C, Kuo J-Y. Pyrolysis characteristics and non-isothermal torrefaction kinetics of industrial solid wastes. Fuel. 2019;251:118-25.

[35] Świechowski K, Stegenta-Dąbrowska S, Liszewski M, Bąbelewski P, Koziel JA, Białowiec A. Oxytree pruned biomass torrefaction: Process kinetics. Materials. 2019;12:3334.

[36] Duan H, Zhang Z, Rahman MM, Guo X, Zhang X, Cai J. Insight into torrefaction of woody biomass: Kinetic modeling using pattern search method. Energy. 2020;201:117648.

[37] Chen WH, Peng J, Bi XT. A state-of-the-art review of biomass torrefaction, densification and applications. Renew Sust Energ Rev. 2015;44:847-66.

[38] Bach QV, Trinh TN, Tran KQ, Thi NBD. Pyrolysis characteristics and kinetics of biomass torrefied in various atmospheres. Energ Convers Manage. 2017;141:72-8.

[39] Di Blasi C, Lanzetta M. Intrinsic kinetics of isothermal xylan degradation in inert atmosphere. J Anal Appl Pyrol. 1997;40:287-303.

[40] Prins MJ, Ptasinski KJ, Janssen FJ. Torrefaction of wood: Part 1. Weight loss kinetics. J Anal Appl Pyrol. 2006;77:28-34.

[41] Nocquet T, Dupont C, Commandre J-M, Grateau M, Thiery S, Salvador S. Volatile species release during torrefaction of biomass and its macromolecular constituents: Part 2 – Modeling study. Energy. 2014;72:188-94.

[42] Repellin V, Govin A, Rolland M, Guyonnet R. Modelling anhydrous weight loss of wood chips during torrefaction in a pilot kiln. Biomass Bioenerg. 2010;34:602-9.

[43] van der Stelt MJC, Gerhauser H, Kiel JHA, Ptasinski KJ. Biomass upgrading by torrefaction for the production of biofuels: A review. Biomass Bioenerg. 2011;35:3748-62.

[44] Bates RB, Ghoniem AF. Biomass torrefaction: Modeling of volatile and solid product evolution kinetics. Bioresource Technol. 2012;124:460-9.

[45] Chen WH, Kuo PC, Liu SH, Wu W. Thermal characterization of oil palm fiber and eucalyptus in torrefaction. Energy. 2014;71:40-8.

[46] Roberts AF. The heat of reaction during the pyrolysis of wood. Combust Flame. 1971;17:79-86.

[47] Bates RB, Ghoniem AF. Biomass torrefaction: Modeling of reaction thermochemistry. Bioresource Technol. 2013;134:331-40.

[48] Yan W, Hastings JT, Acharjee TC, Coronella CJ, Vásquez VR. Mass and energy balances of wet torrefaction of lignocellulosic biomass. Energy Fuel. 2010;24:4738-42.

[49] Na B-I, Ahn B-J, Lee J-W. Changes in chemical and physical properties of yellow poplar (Liriodendron tulipifera) during torrefaction. Wood Science and Technology. 2015;49:257-72.

[50] Nhuchhen DR, Basu P, Acharya B. Torrefaction of poplar in a continuous two-stage, indirectly heated rotary torrefier. Energy & Fuels. 2016;30:1027-38.

[51] Kim Y-H, Lee S-M, Lee H-W, Lee J-W. Physical and chemical characteristics of products from the torrefaction of yellow poplar (Liriodendron tulipifera). Bioresource Technology. 2012;116:120-5.

[52] Silveira EA, Lin B-J, Colin B, Chaouch M, Pétrissans A, Rousset P, et al. Heat treatment kinetics using three-stage approach for sustainable wood material production. Industrial Crops and Products. 2018;124:563-71.

[53] Acharya B, Sule I, Dutta A. A review on advances of torrefaction technologies for biomass processing. Biomass Convers Bior. 2012;2:349-69.

[54] Cai J, He Y, Yu X, Banks SW, Yang Y, Zhang X, et al. Review of physicochemical properties and analytical characterization of lignocellulosic biomass. Renew Sust Energ Rev. 2017;76:309-22.

[55] Sluiter A HB, Ruiz R, Scarlata C, Sluiter J, Templeton D, Crocker D. NREL-TP-510-42618: Determination of structural carbohydrates and lignin in biomass. National Renewable Energy Laboratory. http://www.nrel.gov. [2008-04-25], 16p.

[56] Krasznai DJ, Champagne Hartley R, Roy HM, Champagne P, Cunningham MF.

Compositional analysis of lignocellulosic biomass: conventional methodologies and future outlook. Crit Rev Biotechnol. 2018;38:199-217.

[57] Sheng C, Azevedo JLT. Estimating the higher heating value of biomass fuels from basic analysis data. Biomass Bioenerg. 2005;28:499-507.

[58] García R, Pizarro C, Lavín AG, Bueno JL. Spanish biofuels heating value estimation. Part II: Proximate analysis data. Fuel. 2014;117:1139-47.

[59] Álvarez A, Pizarro C, García R, Bueno JL. Spanish biofuels heating value estimation based on structural analysis. Ind Crop Prod. 2015;77:983-91.

[60] Friedl A, Padouvas E, Rotter H, Varmuza K. Prediction of heating values of biomass fuel from elemental composition. Anal Chim Acta. 2005;544:191-8.

[61] Channiwala SA, Parikh PP. A unified correlation for estimating HHV of solid, liquid and gaseous fuels. Fuel. 2002;81:1051-63.

[62] Cai J, Xu D, Dong Z, Yu X, Yang Y, Banks SW, et al. Processing thermogravimetric analysis data for isoconversional kinetic analysis of lignocellulosic biomass pyrolysis: Case study of corn stalk. Renewable and Sustainable Energy Reviews. 2018;82:2705-15.

[63] Xinjie L, Singh S, Yang H, Wu C, Zhang S. A thermogravimetric assessment of the tri-combustion process for coal, biomass and polyethylene. Fuel. 2021;287:119355.

[64] Huang L, Ding T, Liu R, Cai J. Prediction of concentration profiles and theoretical yields in lignocellulosic biomass pyrolysis. J Therm Anal Calorim. 2015;120:1473-82.

[65] Shen W. An Introduction to Numerical Computation: World Scientific Publishing Company Pte Limited; 2015.

[66] Bansal RK, Goel AK, Sharma MK. Matlab and its Applications in Engineering: Pearson Education; 2009.

[67] Bach QV, Skreiberg O. Upgrading biomass fuels via wet torrefaction: A review and comparison with dry torrefaction. Renew Sust Energ Rev. 2016;54:665-77.

[68] Chen D, Gao A, Cen K, Zhang J, Cao X, Ma Z. Investigation of biomass torrefaction based on three major components: Hemicellulose, cellulose, and lignin. Energ Convers Manage. 2018;169:228-37.

[69] Peduzzi E, Boissonnet G, Haarlemmer G, Dupont C, Maréchal F. Torrefaction modelling for lignocellulosic biomass conversion processes. Energy. 2014;70:58-67.

[70] Sluiter JB, Ruiz RO, Scarlata CJ, Sluiter AD, Templeton DW. Compositional analysis of lignocellulosic feedstocks. 1. Review and description of methods. J Agr Food Chem. 2010;58:9043-53.

[71] Zhou X, Li W, Mabon R, Broadbelt LJ. A critical review on hemicellulose pyrolysis. Energy Technol. 2017;5:52-79.

[72] Prins MJ. Thermodynamic analysis of biomass gasification and torrefaction: Eindhoven University; 2005.

[73] Lange NA, Dean JA. Lange's Handbook of Chemistry: McGraw-Hill; 1999.

[74] Cox JD, Wagman DD, Medvedev VA. CODATA Key Values for Thermodynamics: Hemisphere Pub. Corp.; 1989.

[75] Majer V, Svoboda V, Kehiaian HV. Enthalpies of Vaporization of Organic

Compounds : A Critical Review and Data Compilation: Blackwell Scientific; 1985.

[76] Steele WV, Chirico RD, Knipmeyer SE, Nguyen A, Smith NK. Thermodynamic properties and ideal-gas enthalpies of formation for dicyclohexyl sulfide, diethylenetriamine, dinoctyl sulfide, dimethyl carbonate, piperazine, hexachloroprop-1-ene, tetrakis(dimethylamino)ethylene, n,n'-bis-(2-hydroxyethyl)ethylenediami. J Chem Eng Data. 1997;42:1037-52.

[77] Guthrie JP. Hydration of carboxamides. Evaluation of the free energy change for addition of water to acetamide and formamide derivatives. J Am Chem Soc. 1974;96:3608-15.

[78] Baroody EE, Carpenter GA. Heats of formation of propellant compounds (U), Rpt. Naval Ordnance Systems Command Task 1972. p. 1-9.

[79] Avramescu F, Isagescu DA. Heats of combustion of mono- and difurfurylidene acetone: Revue Roumaine de Chimie; 1978.

[80] Emel'Yanenko VN, Aldona Dabrowska A, Verevkin SP, Hertel MO, Hans Scheuren A, Sommer K. Vapor pressures, enthalpies of vaporization, and limiting activity coefficients in water at 100 °c of 2-furanaldehyde, benzaldehyde, phenylethanal, and 2-phenylethanol. J Chem Eng Data. 2007;52:468-71.

[81] Petitjean M, Reyèspérez E, Pérez D, Mirabel P, Calvé SL. Vapor Pressure Measurements of Hydroxyacetaldehyde and Hydroxyacetone in the Temperature Range (273 to 356) K. J Chem Eng Data. 2012;55:852-5.

[82] Stephenson RM, Malanowski S. Handbook of the Thermodynamics of Organic Compounds: Elsevier; 1987.

[83] Davidovits P. Chapter 10 - Thermodynamics. In: Davidovits P, editor. Physics in Biology and Medicine (Fifth Edition): Academic Press; 2019. p. 137-51.

[84] Atsonios K, Panopoulos KD, Bridgwater AV, Kakaras E. Biomass fast pyrolysis energy balance of a 1Kg/h test rig. Int J Thermodyn. 2015;18:267-75.

[85] Radmanović K, Dukić I, Pervan S. Specific heat capacity of wood. Drvna Industrija. 2014;65:151-7.

[86] Wenzl HFJ. III - The Chemistry of Wood. In: Wenzl HFJ, editor. The chemical technology of wood: Academic Press; 1970. p. 92-156.

[87] Perry RH, Green DW, Maloney JO. Perry's chemical engineers' handbook. McGraw-Hill international editions. 1984.

[88] Rousset P, Aguiar C, Labbé N, Commandré JM. Enhancing the combustible properties of bamboo by torrefaction. Bioresource Technol. 2011;102:8225-31.

[89] Larsson SH, Rudolfsson M, Nordwaeger M, Olofsson I, Samuelsson R. Effects of moisture content, torrefaction temperature, and die temperature in pilot scale pelletizing of torrefied Norway spruce. Appl Energ. 2013;102:827-32.

[90] Mundike J, Collard FX, Görgens JF. Torrefaction of invasive alien plants: Influence of heating rate and other conversion parameters on mass yield and higher heating value. Bioresource Technol. 2016;209:90-9.

[91] Supramono D, Devina YM, Tristantini D. Effect of heating rate of torrefaction of sugarcane bagasse on its physical characteristics. Int J Technol. 2015;6:1084-93.

[92] Lee JW, Kim YH, Lee SM, Lee HW. Optimizing the torrefaction of mixed softwood by response surface methodology for biomass upgrading to high energy density. Bioresource Technol. 2012;116:471-6.

[93] Yan W, Acharjee TC, Coronella CJ, Vásquez VR. Thermal pretreatment of lignocellulosic biomass. Environ Prog Sustain. 2010;28:435-40.

[94] Wang S, Dai G, Ru B, Zhao Y, Wang X, Xiao G, et al. Influence of torrefaction on the characteristics and pyrolysis behavior of cellulose. Energy. 2017;120:864-71.

[95] Dai G, Zou Q, Wang S, Zhao Y, Zhu L, Huang Q. The effect of torrefaction on the structure and pyrolysis behavior of lignin. Energy Fuels. 2018;32:4160-6.

[96] Wang S, Dai G, Ru B, Zhao Y, Wang X, Zhou J, et al. Effects of torrefaction on hemicellulose structural characteristics and pyrolysis behaviors. Bioresource Technology. 2016;218:1106-14.

[97] Biswas B, Pandey N, Bisht Y, Singh R, Kumar J, Bhaskar T. Pyrolysis of agricultural biomass residues: Comparative study of corn cob, wheat straw, rice straw and rice husk. Bioresource Technol. 2017;237:57.

[98] Cui T, Fan W, Dai Z, Guo Q, Yu G, Wang F. Variation of the coal chemical structure and determination of the char molecular size at the early stage of rapid pyrolysis. Appl Energ. 2016;179:650-9.

[99] Felfli FF, Luengo CA, Suárez JA, Beatón PA. Wood briquette torrefaction. Energy Sustain Dev. 2005;9:19-22.

[100] Wang S, Ru B, Dai G, Lin H, Zhang L. Influence mechanism of torrefaction on softwood pyrolysis based on structural analysis and kinetic modeling. International Journal of Hydrogen Energy. 2016;41:16428-35.

[101] Adhikari S, Srinivasan V, Fasina O. Catalytic pyrolysis of raw and thermally treated lignin using different acidic zeolites. Energy Fuel. 2014;28:4532-8.

[102] Kan T, Strezov V, Evans TJ. Lignocellulosic biomass pyrolysis: A review of product properties and effects of pyrolysis parameters. Renew Sust Energ Rev. 2016;57:1126-40.

[103] Peng JH, Bi XT, Sokhansanj S, Lim CJ. Torrefaction and densification of different species of softwood residues. Fuel. 2013;111:411-21.

[104] Phanphanich M, Mani S. Impact of torrefaction on the grindability and fuel characteristics of forest biomass. Bioresource Technol. 2011;102:1246-53.

[105] Sermyagina E, Saari J, Zakeri B, Kaikko J, Vakkilainen E. Effect of heat integration method and torrefaction temperature on the performance of an integrated CHP-torrefaction plant. Appl Energ. 2015;149:24-34.

[106] Gent S, Twedt M, Gerometta C, Almberg E. Theoretical and Applied Aspects of Biomass Torrefaction: For Biofuels and Value-Added Products: Elsevier Science; 2017.